

University of Nebraska - Lincoln

DigitalCommons@University of Nebraska - Lincoln

Computer Science and Engineering: Theses,
Dissertations, and Student Research

Computer Science and Engineering, Department of

8-8-2012

AUTOMATION OF LANDMARK SELECTION FOR RODENT BRAIN MRI- HISTOLOGY REGISTRATION USING THIN- PLATE SPLINES

Ayan Sengupta

University of Nebraska-Lincoln, uam111@gmail.com

Follow this and additional works at: <http://digitalcommons.unl.edu/computerscidiss>



Part of the [Computer Engineering Commons](#), and the [Computer Sciences Commons](#)

Sengupta, Ayan, "AUTOMATION OF LANDMARK SELECTION FOR RODENT BRAIN MRI-HISTOLOGY REGISTRATION USING THIN-PLATE SPLINES" (2012). *Computer Science and Engineering: Theses, Dissertations, and Student Research*. 45.
<http://digitalcommons.unl.edu/computerscidiss/45>

This Article is brought to you for free and open access by the Computer Science and Engineering, Department of at DigitalCommons@University of Nebraska - Lincoln. It has been accepted for inclusion in Computer Science and Engineering: Theses, Dissertations, and Student Research by an authorized administrator of DigitalCommons@University of Nebraska - Lincoln.

AUTOMATION OF LANDMARK SELECTION FOR RODENT BRAIN
MRI-HISTOLOGY REGISTRATION USING THIN-PLATE SPLINES

by

Ayan Sengupta

A THESIS

Presented to the Faculty of
The Graduate College at the University of Nebraska
In Partial Fulfillment of Requirements
For the Degree of Master of Science

Major: Computer Science
Under the Supervision of Professor Ashok Samal

Lincoln, Nebraska

May, 2012

AUTOMATION OF LANDMARK SELECTION FOR RODENT BRAIN
MRI-HISTOLOGY REGISTRATION USING THIN-PLATE SPLINES

Ayan Sengupta, M.S.

University of Nebraska, 2012

Advisor: Ashok Samal

Image registration is the process of aligning two different images of the same object taken at different times, at different orientations or using different instruments. This is common in medical applications since multiple modalities are used to image different parts of the body. This is an important early step in many diagnostic procedures such as change detection, monitoring tumor or quantifying spread of a disease. The widely used landmark based registration approach is tedious, time consuming, inconsistent and error prone. Furthermore, the standard schemes based on rigid and affine transformation can only describe global geometric differences between the objects of interest. In the medical domain, local variations and changes are common due to natural, instrument, surgical and patient induced distortions. Such effects can be accommodated by elastic or non-linear schemes.

Thin-plate spline warping is a non-linear technique that is widely used for registering different types of medical images including magnetic resonance and histology images. However, this technique is constrained by manual landmark

selection. In this research, we have developed a method to automate the landmark selection process using thin-plate splines by maximizing the normalized mutual information between the two images. The approach has been studied in the context of registering MRI images and the histological sections of a rodent brain. The approach involves using level-set evolution to isolate the brain in a volumetric MRI image. Then the MRI volume is registered to the corresponding 3D histology (stacked histological sections) image using an affine transformation. The MRI volume is then re-sliced to match the corresponding histological sections. Finally these 2D MRI slices are warped to the histological sections using thin-plate splines maximizing the normalized mutual information. The approach was tested with images from 4 rodent brains with over 170 MRI images and over 120 block face images for each brain. The effectiveness of the landmark was determined by comparing its performance with the results manually obtained by three experienced technicians. The results show that the landmarks obtained using the NMI optimization approach is effective and comparable to manual extraction results.

ACKNOWLEDGEMENTS

I would like to acknowledge the advice and guidance of my advisor, Dr. Ashok Samal. He has been more than a mentor to me guiding me throughout my entire time in the Department of Computer Science and Engineering in University of Nebraska, Lincoln. I sincerely thank him for introducing me to the research of Medical Image Processing.

I thank Dr. Yutong Liu of University of Nebraska Medical Center, Omaha for playing a pivotal role in this project. He was always there to extend all kinds of help and support to understand the medical science problem and providing me the required background and all the experimental data for my work.

I sincerely acknowledge the support and encouragement of all of my friends and family members without which I wouldn't have been able to finish my degree. Moreover, I would like to thank all the staff of Computer Science and Engineering for providing me essential informations about the program which helped a lot in planning and pacing my work.

*This thesis is dedicated to my mom and dad and to the special friend who
always stood by me in each and every step of my life*

Contents

1	Introduction	1
1.1	Medical Image Registration	4
1.2	Applications	6
1.3	Objectives and Research Contributions	10
1.4	Thesis Outline	11
2	Related Work	12
2.1	Medical Image Segmentation	12
2.2	3D Volume Reconstruction and Alignment	19
2.3	Image Registration Principles	20
3	Approach	23

		7
3.1	Problem Definition	23
3.1.1	Brain Extraction from MR images	26
3.1.2	Image Warping for Nonlinear MRI-Histology Registration	28
3.2	Level-Set in Brain Extraction on MRM	30
3.2.1	Introduction	30
3.2.2	Motivation	31
3.2.3	Theory	32
3.2.4	Level Set segmentation	38
3.3	Blockface Image Segmentation	48
3.3.1	Histogram Equalization	48
3.3.2	Canny Edge Detector	50
3.3.3	Blockface Image Segmentation	51
3.4	Alignment	60
3.5	Registration approach and Optimization	63
3.5.1	Thin Plate Spline Warping	63
3.5.2	Automation of Landmark Selection, Registration and Optimization	65

	8
4 Results and Evaluations	72
4.1 DataSets	74
4.1.1 MRI slices	74
4.1.2 Blockface and Histological Images	75
4.2 Results	77
4.3 Evaluation	84
5 Summary and Future Work	90
Bibliography	93

List of Figures

3.1	Flowchart of the MRI and histology co-registration procedure. Texts without boxes represent data; boxed texts represent data processing procedures. Arrows entering a box represent input for transformation.	26
3.2	Brain extraction using a level set method. A: Selection of constrain contour on one sagittal slice and B: two axial slices. C: Constrain points defined on coronal slices from contours are D: used to automatically define a starting contour. E-F: Resulting brain extraction	28
3.3	Image warping using thin-plate splines with landmark optimization. Contours of the brain boundary and corpus callosum were manually traced on the MRI (A) and histology (C) to generate landmarks. Similarly, corresponding contours on the blockface were traced to generate the homologues of the landmarks (B). (D, E): The warped MRI slice (D) and histological slice (E) using thin-plate splines. BMM clusters appear on the MRI image (black line) (A and D) and on the histological section (blue line) (C and E).	30
3.4	Connective tissues around the brain	32
3.5	The whole head MRI slice from which the brain is segmented	39
3.6	Original Histogram of the Image	40
3.7	Modified Histogram of the Image	40

	10
3.8 The Gaussian Smoothing Filter	41
3.9 The Convolution of the original Image and the Gaussian Filter . . .	42
3.10 The Edge Indicator Function	43
3.11 The Evolution of Level Set Function: (a) after 50 iterations (b) after 200 iterations (c) after 500 iterations (d) after 1500 iterations	44
3.12 The Evolution of Level Set Contour: (a) after 50 iterations (b) after 200 iterations (c) after 500 iterations (d) after 1500 iterations	45
3.13 The Final Segmented Image of the Brain from the initial image . . .	45
3.14 The Evolution of 3D Level Set volume curve: (a) after 1 iteration (b) after 15 iterations (c) after 80 iterations	47
3.15 Blockface Image of the brain fixed in paraffin	52
3.16 Region of Interest in the Blockface Image slice	53
3.17 Gaussian Kernel	54
3.18 Edge Indicator function used in segmenting the blockface image . .	55
3.19 Affine Transformation of the blockface image slices: (a) Translation (b) Rotation	56
3.20 Final Segmented image of the blockface Images	57
3.21 The Evolution of 3D Level Set volume curve: (a) after 1 iteration (b) after 15 iterations (c) after 80 iterations	59

	11
3.22 MRI histological pair of images to be registered: (a) Low resolution T ₁ -wt MR image (b) High resolution stained Histological image . . .	68
3.23 (a) Logical BW representation of T ₁ -wt MR image (b) Logical BW representation of histological image	68
3.24 (a) Canny Edge detection of T ₁ -wt MR image (b) Canny Edge detection of histological image	69
3.25 (a) Initial 5 landmarks determined on T ₁ -wt MR image (b) Initial 5 landmarks determined on histological image	69
3.26 Final Warped image after the co-registration is completed. NMI index is 0.69	70
3.27 The initial landmark set(yellow) and optimized landmark set(blue)	71
3.28 Visible similarity between the warped and histological image observed from the superimposition of the 2 images	71
4.1 MRI volume:(a) Coronal view, (b) Sagittal view, (c) Axial View . . .	75
4.2 Blockface Image of the brain fixed in paraffin	76
4.3 Histological Image slice	77
4.4 Level Set Evolution Application: Column(a) Whole head MRI slices Column(b) Corresponding segmented brain sections	78
4.5 Blockface Image segmentation: Column(a) Blockface image slices Column(b) Corresponding segmented and affine transformed brain sections	79

	12
4.6 Poor Blockface Image segmentation examples	80
4.7 Representation of MRI and Blockface volume	81
4.8 Representation of 3D aligned volume	82
4.9 Representation of MRI and Blockface and 3D aligned slices	82
4.10 Thin Plate Spline(TPS) warping results of three MRI-Histological Slice pairs	83
4.11 Comparison of Warped Images obtained from Manual Landmarking Methods and Automatic Landmarking Methods of Brain Slice 1 . . .	85
4.12 Comparison of Warped Images obtained from Manual Landmarking Methods and Automatic Landmarking Methods of Brain Slice 2 . . .	86
4.13 Comparison of Warped Images obtained from Manual Landmarking Methods and Automatic Landmarking Methods of Brain Slice 3 . . .	87
4.14 Comparison of Normalized Mutual Information of Warped Brain Slice and Histological sections	89

List of Tables

3.1	Principle steps of the Automated Image Processing Technique	25
3.2	Pseudocode of the algorithm for MRI-histological slice registration .	67
4.1	Comparison of Target points on the Histological Image and Warped Points obtained from Experiment for particular Source Points (Set1)	87
4.2	Comparison of Target points on the Histological Image and Warped Points obtained from Experiment for particular Source Points (Set2)	88
4.3	Comparison of Target points on the Histological Image and Warped Points obtained from Experiment for particular Source Points (Set3)	88
4.4	Comparison of Normalized Mutual Information of Warped Brain Slice and Histological sections	88

Chapter 1

Introduction

It is a popular saying that "A picture is worth a thousand words" which conveys the immense amount of data contained in an image. In the previous few years the image acquisition techniques have improved by leaps and bounds, leaving a wide and unexplored field of image data which is yet to be analyzed and understood fully. Image analysis principles have become indispensable to cope with the growing amount and the diversity of images obtained. Over the years a broad range of techniques have been developed to understand various types of image data and problems. An important problem in image analysis is the problem of image registration.

Image Registration is the process of overlaying two or more images of the same object taken at different time, from different viewpoints or with different scanners or sensors[51]. The main problem arises when these images taken at

different time/viewpoint or with different scanners need to be compared. These images need to be aligned to one another so that the differences can be determined. These differences in these images arise due to difference in imaging conditions. Image registration geometrically aligns two images - the reference and the sensed image and hence serves as a crucial step in image analysis technique. In any image analysis technique the determination of final information involves other related processes as combination of various data sources like in image fusion, change detection and multichannel image registration. Image registration is used extensively in medical image analysis. For example, Computed Tomography (CT) images of a certain region of the body yields high contrast image of the local bone structures and calcification. On the other hand MRI image of the same region shows high soft-tissue contrast.[29, 18] In this case for proper diagnosis of the disease and also designing the therapy require information from both the CT and MRI image modalities. In order to do the comparative analysis of both the images and to gain more complete knowledge about the same part of the body being imaged, image registration provides a powerful, accurate and automatic tool. Image registration has widespread applications in various fields like remote sensing, environmental monitoring, weather forecasting, and geographic information systems (GIS). In medical science the application of image registration is extensive in multimodal image analysis like combining computed tomography (CT) images with magnetic resonance imaging (MRI) to obtain more complete information about the patient health, tracking growth of diseases or tumors, determine therapeutic solutions and also for comparing specific patient's data with anatomical atlases.

One of the key research goals in image registration is to find identify the variations in the images. The type of variation guides the choice of the

registration techniques. There are three major types of variations.[51] The first type of variation arises from differences in acquisition which make the images misaligned. In order to reduce the deformation of these images a global spatial transformation model is typically used. The optimal transformation required for this registration is determined by knowledge of the factors which caused the deformation. The second type of variation between two images originates from the different conditions during acquisition of the images. These differences in conditions can be diverse, e.g. lighting and atmospheric conditions, which are often difficult to model. The difference in ambient conditions during image acquisition results in difference in image intensity values, but may differ in spatial orientations such as perspective distortions. The third type of variation is found when the regions of interest in the images are under motion, growth or other changes. Image registration principles in general are not used for the second and third type of image variations but these variational effects make the process of registration difficult to implement. Specifically, in the third type of variation where the region of interest (ROI) is under motion or growth, it is the variation of the images which contains the information about the ROI; hence registration is not used to remove the deformations. Image Registration consists of several processes; in general image registration can be represented as combinations of the following[18]:

1. a feature space,
2. a search space,
3. a search strategy, and
4. a similarity metric.

The *feature space* consists of those ROIs or features in the image which are used for matching. The *search space* consists of those features with which the correspondence of the feature space is searched and determined. The *search strategy* determines how to find and model the transformation of the feature space to the search space. The *similarity metric* determines the correlation of the registered image and the target image and is the index of how closely these two images match. The general algorithm for image registration is to continue the search until a predetermined satisfactory value of similarity measure is obtained.

1.1 Medical Image Registration

The increasing use of radiological images in healthcare and medical research has made a radical impact on medical science and disease therapy. Use of medical imaging techniques provides the clinician an increasingly multifaceted view of brain function and anatomy. In most cases medical images are complimentary which means that they convey different sets of data about the same organ taken at different time or by different modalities.

It is important to be able to accurately relate information in the multiple images taken for diagnosis, treatment and basic science. Registration plays a central role in this process. It is extensively applied in combining images of the same subject from different modalities, aligning temporal sequences of images to compensate for motion of the subject between scans, image guidance during interventions and aligning images from multiple subjects. Radiological image

acquisition systems are not efficient enough to produce images which can convey all the information that a physician needs for accurate diagnosis. In this context efficient medical image registration becomes indispensable because it provides benefits by extracting information after accurately aligning the images, and visualizing the aligned images. For example, the structural orientation and anatomy of different parts of the brain are exquisitely demonstrated by several imaging techniques such as X-ray, computed tomography (CT) and magnetic resonance (MR) imaging. Complimentary image information can provide comprehensive knowledge about the concerned organ to physician and hence clinical diagnosis and therapy planning are increasingly based on these data[51]. Traditionally physicians used to interpret data from different modalities recorded at different times using poorly described manual alignment which involves applying some spatial transformation between structures within the image pair, but it resulted in poor visual quality of the aligned images. Based on their previous experience the physicians can generally understand the poorly aligned images and decipher important information. But there is a need for automated and objective methods of aligning and quantifying image information. Registration of information of one image to the information of another image involves the establishment of a one-to-one mapping between the points in each image. The mapping can be partial or complete, but it must include all points of diagnostic or surgical interest to be useful.

As defined earlier, the term registration means the determination of a transformation from one image space to another. The image pair is considered to be registered when the transformation is entirely determined considering the pre-determined similarity metric. For easier comparison of multimodal images

the registration techniques are used to superimpose features from one imaging study over those of another study. For example, registration can be used to overlay skeletal structures and areas of contrast enhancement seen in CT images and soft-tissue anatomy as seen in MR images thus making the final registered image more complete and informative. Similarly, functional activities of the brain as scanned by PET can be viewed in the context of brain anatomy imaged with MR giving a clear indication of localization of certain activities in particular sections of the brain. Sometimes, growth of disease, tumors and other structural changes of a particular organ with respect to time needs to be logged. In that case same modality image of the same organ is taken at different times and registration algorithms are utilized for comparative monitoring of serial images for the purpose of quantitative comparison, which increases the precision of treatment.

1.2 Applications

Medical image processing has widespread application in medical science. With increasing accuracy of imaging systems, higher resolution and contrast of in-vivo imaging has made medical image processing an indispensable part. Among the varied application of different image processing techniques in medical science, here we are mentioning only some of them. Mammography is an imaging process of human breast for diagnosis of breast cancer. It is perhaps the most reliable technique to determine the lesions in the breast. The image quality of the mammograms is severely affected by factors like luminance, ambient light etc. which may result in false negative cases, which means that the patient had cancer but she was

detected to be negative. Medical image processing techniques are applied to make the process of mammography more error free. Image enhancement techniques can significantly improve the quality of the acquired mammogram, image registration techniques provides an important tool to quantify the growth of the disease and its present situation. CT and MRI imaging techniques are extensively used in neuroimaging problems. Medical image processing technique can be used to study the flow processes of the brain, such as flow of information, energy, chemicals, drugs etc. which is an approximate indication of brain activity. Synchronization of MRI, fMRI, Conductivity tensor imaging (CTI) and EEG is used to map the electrical dipole source of epileptic firing focus deep inside brain, different behavioral stages of Alzheimers disease can also be determined in this process. It is evident from this discussion how broad and diverse is the application of medical image processing techniques. In our project we developed an image processing technique to quantify the growth of HIV related neurocognitive disorders in rodent brain and also an automatic point-landmark selection system in co-registering the MRI and histological image slices. It is described in details in the following paragraphs.

In the advanced stages of HIV-1 infection, a spectrum of neurological dysfunctions termed as HIV-1 Associated Neurocognitive Disorders (HAND), are associated. In the most severe cases, HAND can be correlated pathologically to multinucleated giant cell called the HIV-1 Encephalitis (HIVE)[25, 26, 32]. Currently, there are Magnetic Resonance Imaging (MRI) methods to diagnose different kinds of neurological dysfunctions. But, they haven't been designed specifically to diagnose HIVE and HAND. Biomarkers to visualize disease progression and treat it are not available currently. In case of diseases like HIV, cancer etc. early detection of the disease serves as a very important step towards the therapy of

the disease. In order to do that the first thing we need to determine is the quantification of the growth of disease in a subject. In this case to understand the pathological procedure of HAND and to develop effective therapies to improve the life quality of AIDS patients, murine models of HIVE and HAND are developed. Non-invasive ultra-high spatial resolution MRM with relatively short scan time is a good indicator of the disease progression. As the brains of the Murine Models are stained with manganese we can make use of the Manganese Enhanced multispectral Magnetic Resonance Microscopy (MEMMRM) technique to detect different structures and neuronal viability. Multispectral MRI provides significantly enhanced anatomical details and indications of pathology in HIVE and HAND compared to standard MRI techniques. In order to determine a non-invasive technique to diagnose the progress of the disease and treat it accordingly, a correlation between the MEMMRM results and the histologically images could be achieved. Image processing techniques could be developed such that given a MEMMRM (MRI) and the histological image of a HIV-1 infected mice brain, the process of co-registering the MEMMRM (MRI) and the histological images could be automated.

By successfully implementing the co-registration between the MEMMRM (MRI) images and the histological images, a non-invasive method to diagnose the disease could be made possible. The image segmentation and co-registration techniques are intensively necessary in biomedical applications to validate imaging results with the histological analysis. The project would provide a valuable analysis of efficient implementation of the image segmentation and co-registration techniques particularly for HAND. Initially, landmarks are being selected on the MRI source image and the histological target image. They can be done manually

but the process is tedious and error-prone. Using these landmarks, the source image is being warped on to the target image. Among the various warping techniques, thin-plate splines algorithm is used in this application because it has been widely accepted as in medical imaging as a powerful warping tool[23, 30].

The study of HIVE and HAND requires quantitative analysis of the growth of the disease in the infected mouse brain and in order to do that developing image processing algorithm is indispensable because the manual methods are always error prone and tedious. MEmMRM provides lots of mutually supplemental information and hence stands out as a powerful tool in neuroscience research in small animals. Processing the data produced by MEmMRM and deciphering important information out of it are the major applications of the Image processing algorithm developed in the study. In modern biomedical applications the areas of intensive research are Image segmentation and image co-registration principles. The Image processing algorithm not only automates the process of quantification of the growth of the disease and removes human errors, but also validates imaging results with the histological analysis. To round up in this project image processing principles are used extensively to simulate the process of brain extraction from the skull(skull stripping from the MRI image), 3D affine alignment of MRI volume and Blockface volume of the same brain, automatic selection and optimization of landmarks for non-linear co-registration of MRI and histological section, calculation of Normalized Mutual Information (NMI) of MRI and histological sections and evaluating the results against manual methods. The greatest advantage of this method is that it makes the entire process non-invasive. As it is a well-known fact that histology is used for tissue structure analysis also, the image processing algorithm used here has the potential to be applied in in-vivo histology analysis in

future.

1.3 Objectives and Research Contributions

The goal of this research was to develop an approach to register MRI images to corresponding histological image sections of rodent brain. The specific contributions of this image processing research can be enumerated as following:

1. The segmentation of brain from whole head MRI of the rat brain. A major section of the analysis was done to adapt and fit the traditional Level-set segmentation algorithm for segmentation of the brain (ROI) from the whole head MRI image slices.
2. The 3D affine alignment of the blockface volume and the MRI brain volume thus reducing the global distortion of the brain occurred due to physical slicing the brain while doing the histological analysis. I developed the segmentation algorithm of the blockface images, stacking them up to form the blockface volume and applying the demon-registration algorithm for affine 3D registration of the MRI volume and the Blockface volume.
3. The main section of the research is dedicated towards developing automatic landmark selection procedure and the optimization of these landmarks based on Normalized Mutual Information. In process of that the non-linear co-registration principle of Thin Plate Spline warping technique is explored in details. The landmark sets used for this non-linear co-registration is selected

automatically and they are optimized along the brain edge by an iterative method of minimizing a definite cost function which in turn maximizes the Normalized Mutual information between the pair of images (MRI-histological image pair).

4. The evaluation of the automatic landmark selection and co-registration procedure against manual methods of co-registering.

1.4 Thesis Outline

The rest of thesis is organized as follows. Chapter 2 deals with the previous researches which are specific to our research, i.e. medical image registration. Chapter 3 explains in details our research approach, the specification of our algorithms and the implementation strategies. Chapter 4 describes the dataset used for our research and the results obtained using our approach. The results are compared with those obtained by trained professionals in this field. Chapter 5 gives a summary and directions for future research.

Chapter 2

Related Work

In this chapter, we describe previous work related to our research. In particular, we describe (a) the problem of image segmentation, with a focus on medical images, (b) alignment of 3D point clouds and (c) registration with landmarks.

2.1 Medical Image Segmentation

Segmentation is highly used technique in computer vision to isolate regions of that are meaningful to the application and easy to analyze. The body of literature in segmentation is vast and a complete summary is beyond the scope of the thesis. Interested readers can see . Segmentation is an important problem in medical image analysis since many imaging mechanisms like CET and MRI offer

high resolution in-vivo structure of organs and identifying them accurately can greatly assist clinical diagnosis. There are a lot of diverse algorithms available for successful image segmentation for common applications but the application of dedicated algorithms for Medical Image processing requires more concrete application background. Medical Image segmentation can be successfully performed only when we have a prior knowledge like the imaging procedure or the biomechanical behaviors of organs or structures and that can be crucial for a successful segmentation. Due to the intrinsic noise and the partial volume effect (Zaidi, 2005) Medical image processing algorithms should be sophisticated enough to handle the segmentation task. The present day medical image processing algorithms incorporate successful implementations of modern mathematical and physical techniques and have considerably enhanced the accuracy of the segmentation. We briefly summarize the most widely used segmentation techniques in medical image analysis. These algorithms are classified into three categories: algorithms based on threshold, algorithms based on pattern recognition techniques and algorithms based on deformable models. A very important point that needs mention in this context is that, often it is found that the algorithm utilizes concepts from all of the previously classified categories to achieve satisfactory segmentation depending on the type and properties of the image to be segmented.

Threshold based Approaches : Algorithms that segment based thresholding make the assumption that region of interest in the image can be discerned by quantifiable features, like intensity or gradient magnitude. Thus a pre-determined or dynamically generated threshold is used to filter the intensity or gradient image to remove the redundant information. In these algorithms, segmentation is done

based on finding those pixels which satisfy the threshold constraints. Determination of threshold is the most critical and key part of these algorithms. Thresholds are either of the following two ways. Manual Threshold: In this method the threshold of segmentation is determined manually by prior knowledge of the image and its pixel value distribution over the area. Automatic Threshold: The threshold for segmentation is determined automatically in an iterative manner, gathering information about the pixels in the image. The threshold based algorithms can be further divided into edge-based segmentations, region-based segmentations and hybrid segmentations.

Edge-based segmentation algorithms use threshold values relating to the edges of different objects in the image. Actually the objects in the images are represented and depicted by their edge points. The edge-based algorithm tries to determine the edge pixels based on the threshold constraint and filters the other pixels as noise. There are lots of edge detection algorithms present, out of which the Canny edge detection algorithm (Canny, 1986) and Laplacian edge detector are the more popular and efficient. Canny edge detector algorithm finds the gradient of the image, object edges are expected to have higher gradient magnitude than the rest of the image. Hence it uses a threshold of the gradient magnitude to find the potential edge pixels. It is to be noted that the edge-based algorithms tend to find the discrete edge pixels only, therefore the segmented edges in most cases are discontinuous or incomplete. Some post processing of the segmented image has to be done to Connect the breaks or eliminate the holes.

The region-based segmentation algorithm is based on the observation that pixels intensities inside a structure are more or less of similar magnitude. In a

typical region growth algorithm (Adams and Bischof, 1994) the based on prior knowledge of the position of the structure to be segmented the seeds (few pixels) are determined and a threshold of intensities is defined. Then the neighboring pixels are added to this region maintaining the threshold interval thus resulting in the growth of the region. The success of this method depends on the accuracy of critical procedure of determining the seeds and the interval of threshold intensities. In order to get away with it automatic methods involve statistical analysis of the image and prior knowledge about the image. The accuracy of segmentation of CT and MR images is improved considerably by introduction of homogeneity criterion (Pohle and Toennies, 2001) which made the region growing algorithms adaptive to the different locations of initial seeds. One of the prime drawbacks of the threshold based segmentation approaches is that it relies entirely on image intensities, and hence these methods are not equipped enough to handle the partial volume effects. Due to the intrinsic noise and partial volume effect the edges of structures/organs in medical images are often not well defined. For that reason only threshold based segmentation approach has limited application in medical image segmentation, they are mostly used in conjunction with other sophisticated methods.

Segmentation approach based on pattern recognition : A pattern is an entity which can be associated with a definite name. Pattern recognition algorithms deal with grouping and classifying of a set of data into different patterns. (by E. Micheli-Tzanakou (Boca Raton, FL: CRC, 2000, 371 pp., ISBN 0-8493-2278-2).Reviewed by Ke Chen.) The main application of pattern recognition algorithms is feature extraction and classification. There can be two different schemes of pattern recognition algorithms namely, supervised and unsupervised schemes.

Supervised algorithms tend to classify the dataset and classify and associate the data to pre-defined classes (also known as classifiers). In unsupervised scheme there are no pre-defined data classes and hence this algorithm targets to classify the input data into different clusters based on some similarity measure. These clusters are later defined to be classes. The segmentation algorithms based on pattern recognition treat the structures in the medical images as patterns. Among all other pattern recognition techniques the most applied ones in medical image segmentation are supervised or unsupervised classification algorithms.

Pattern recognition algorithms are used extensively in medical image segmentation problems. Artificial neural network (Alirezaie, et al, 1997), support vector machine (Wang, et al 2001) and active appearance models (Cootes, et al, 2001) are the better known supervised classification algorithms used in Medical Image segmentation. In order to determine the pre-determined classifiers a training dataset is required. In some algorithms like supervised artificial neural networks (ANNs) and support vector machines (SVMs) non-linear statistical data modeling is used. The weights in each classifier is determined through optimized energy functionals and updated after processing of each sample in the training set. Training sets are used to determine the mean shape, mean appearance and ranges of shape parameters hence it is an important and critical aspect of the entire pattern recognition process. Moreover some restrictions are laid down to make the segmentation of the image follow a definite shape and pattern and hence the amount of similarity of the segmented image and the original image can be maintained at a certain level. Supervised pattern recognition algorithms produce very satisfactory results in medical image segmentation problems. This method is found very effective in segmenting cardiac and brain images.

Unsupervised pattern recognition algorithms are also used frequently in medical image segmentation where the classifiers cannot be determined from prior knowledge of the image. Unsupervised algorithms are popularly known as clustering algorithms because they can determine the clusters themselves without any training sets and the structure features in the image are determined from the classified points itself. FCM algorithm is commonly used in segmentation of MR images and transmission images (Mohamed, et al, 1998). The idea behind this FCM algorithm is derived from the extensively used K-means clustering algorithm where K is the predetermined number of clusters. The segmentation of the image is achieved by labeling different parts of the image based on their respective membership in K different clusters. The membership of a particular pixel in a cluster is determined by its Euclidean distance from the cluster centroid, the cluster centroids are updated iteratively when a new pixel is added to it. The algorithm ends when all the pixels in the image are assigned to each of the K clusters. Iterative Self-organizing Data Analysis Technique Algorithm (ISODATA) is based on the same idea driving the FCM algorithm; the only difference is that the number of clusters is not pre-determined but dynamically generated. These unsupervised clustering algorithms have yielded good results in segmentation of Positron Emission Tomography (PET) scans where it is applied to segment different types of tissues and blood. Other popular unsupervised algorithms in medical image segmentation field are unsupervised neural networks like Hopfields neural network (Cheng, et al,1996). Template matching algorithms and atlas-guided algorithms are other important medical image segmentation algorithms which need prior knowledge of the image for its successful implementation (Gindi, et al, 1993; Akselrod-Ballin, et al, 2006).

Deformable templates : Another popular approach towards shape analysis is based on deformable models which are more flexible and can be used for complex segmentations. The procedure of this algorithm can be viewed as study of active contours and modeling evolution of the contour. Based on the representation of the contour the deformable template models can be classified as parametric models and geometric models. Parametric models have been inspired from the concept of Snake Method (Kass, et al, 1987). In this model the contour is sampled at a certain interval and those sampled points are the points of interest when the contour is moving. The evolution of the contour is defined by energy functionals which are actually a combination of two terms, namely the internal and external energy. The internal energy is defined as the geometric properties of the contour like the length, area and curvature etc. The external energy pulls the contour outside so that it can take the proper shape and position and it is defined by image information. An Euler-Lagrange equation is defined which states position of the contour under proper balancing of both the internal and external energy functions. The position of the moving contour at any point of time is actually the object boundary.

The parametric deformable model has an intrinsic disadvantage, which is known as the topological constraint. As a result of that the curve cannot properly approximate the boundaries of not properly connected components. In order to get over this disadvantage the geometric deformable models are developed which are based on the level set methods (Osher and Sethian). This model incorporates the concept of implicit snake method [2, 12] as opposed to the explicit snake method used in the parametric model. In this model the initial curve is approximated as the zero level curve of a Snake function. The evolution of the curve is determined by partial differential equations. As a result it is not required to track sampled

contour point. The topological changes are implicitly handled because the contour equation is embedded as higher dimensional level set functions. In this project we have used level set evolution technique to segment the brain from the whole head skull MRI images.

2.2 3D Volume Reconstruction and Alignment

The problem of 3D volume reconstruction and medical cross section registration is considered a challenging problem in medical image processing and has been extensively studied. The goal of 3D volume alignment is to form a high resolution 3D volume from a set of spatial tiles (high-resolution 2D images or 3D cross section volumes). Literature in determining the accuracy and computational complexity of 3D alignment techniques is rather scarce. The related work in this field has been from computer vision which deals with matching and alignment from points and frames while modeling rigid motion of objects. A researcher performing 3D alignment problem has to decide on some very critical factors like the image size used in the registration, transformation models (rigid, affine or elastic) or whether the registration process is to be manual, semi-automatic or fully automatic.

Thirion introduced a registration algorithm called 'demons algorithm for 3D registration based on pixel velocities caused by edge based forces and is similar to fluid registration . This method of 3D alignment has high registration precision and it has been used extensively in medical image processing. The main application it has been used is for 3D registration of MRI volumes. However this

method is not directly applicable to register 3D image volumes obtained from different modalities. In our research we use the 3D alignment of MRI volume and the blockface volume. This algorithm is modified for our application.

2.3 Image Registration Principles

Image registration is a well-known technique which is used extensively in establishing one to one correspondence between images of the same scene taken at different time or at different viewpoints or with different sensor, scanner, other modalities etc. One of the most interesting applications of image registration is in medical imaging where it is effectively used in fusion of medical images like PET-MRI, CT-PET and many more. To register two images the geometric transformation between the pair is calculated which determines the alignment of the source image with respect to the reference image. The most common image registrations are namely rigid, affine, projective, perspective, global and elastic.

Image registration algorithms can be classified based on modality, intensity or methods for registration. Some important registration algorithms and their respective basis of registration are discussed here. In **pixel based registration** cross-correlation is the basic statistical approach used. It is used for template matching or pattern recognition in a particular picture where location and the orientation of a template or pattern is determined. **Feature based registration** makes use of image features derived by feature extraction algorithms and thus reduce the redundant information during registration. Therefore in this approach

the unique features which are likely to be found in both images and are tolerant of local distortions are selected for registration. After feature extraction, control points in the reference image are matched with feature points and then spatial mapping is performed on the image pair to get the registration information. **Contour based registration** uses high statistical features for matching image feature points. The characteristic concept of this registration is the extraction of region of interest from the image using color image segmentation principle.

Image registration based on point landmarks is a very important and widely used approach. Several schemes are used for point landmark based registration, e.g. rigid, affine and elastic schemes. Of these schemes the elastic scheme is more important in medical imaging because it is non-linear and is better known as warping . The geometric global differences between two images are described by rigid and affine transforms but the elastic schemes also deal with local differences. In medical image registration several deformation factors like difference in anatomy (or pathology), scanner or patient induced distortions, as well as intraoperative deformations due to surgical interventions need to be considered. Hence the local geometric differences considered in the non-linear/ elastic registration scheme is more suitable for this application. The most widely used point-landmark based elastic registration is **Thin Plate Spline registration**. This approach was introduced in medical image analysis by Bookstein. Evans et al. applied this scheme to 3D medical images. Alternative splines based on the Navier equation, which have been named elastic body splines, have recently been introduced by Davis et al. Extensions of point-based elastic schemes which allow inclusion of additional attributes at landmarks have been proposed by Bookstein et al. The combination of thin-plate splines with mutual information as similarity

measure for the purpose of refining initially coarsely defined landmarks was first proposed by Meyer et. al.

In all the registration approaches mentioned above the interpolation case has been considered, which means that the corresponding landmark set are assumed to match exactly. It implicitly means that the exact position of the landmarks is known and has to be specified precisely for doing this TPS registration. This assumption is unrealistic because landmark extraction is always error-prone. Hence the need for approximation based landmark selection schemes needs to be developed. Bookstein proposed a process of relaxation of initial landmarks incorporating several energy terms, where a term represents the bending energy of interpolating thin plate splines and the other term represents the distance of landmark configurations. This approach incorporates both isotropic and anisotropic error. This approach is not related to a minimizing functional with respect to the searched transformation. Recently Christensen et al. introduced another approach for non-linear registration which has a hierarchical approach to image registration combining landmark based scheme with a fluid model.

Chapter 3

Approach

3.1 Problem Definition

Medical image registration serves as an important tool to build up a comparative study between the images of the same organ taken at different time, or different point of view or different scanners. In order to directly compare in-vivo MRI images with histological slices the application of image co-registration is necessary. It should be kept in mind that the MRI procedure is in-vivo which means that the brain is intact in its position inside the skull, on the other hand the histological slices are produced by physically dissecting the brain, fixing it in paraffin and slicing it. Therefore it is expected that the histological slices are quite deformed than the actual in-vivo MRI slices. The success of MRI-histology co-registration

depends on the accuracy of both global and local alignment of the histological and MRI slices. To determine the global deformations resulting from brain removal from skull and tissue fixation, as well as the slice specific deformation caused by tissue tearing and distortion during histological processing is definitely a challenge that is addressed in this project. Direct co-registration of the MRI and histological images is feasible but its computational complexity is very high, has to deal with lots of parameters defining the actual deformation and also very error-prone. In order to get past this technical challenge an intermediate imaging system is developed. In the process of intermediate imaging either ex-vivo MRI of the brain volume is obtained or in other cases digital images are obtained during cryosectioning (slicing the brain fixed in paraffin). In our project the second approach is taken and the cryosectioning of the brain at an interval of $150\mu\text{m}$ is done and the digital images thus produced are known as the blockface images. The blockface image slices can be stacked up in 3D producing the entire brain volume and it acts as a spatial reference which helps in compensating the global deformation factors encountered during the MRI and histological co-registration. The complex registration process is simplified by first registering the MRI brain volume to the intermediate reference to compensate for the global deformation, and then warp the corresponding registered MRI-histology sections to correct slice specific deformations (81-84). It is worth mentioning at this point that the introduction of intermediate imaging system simplifies the MRI-histology co-registration but the two critical problems addressed in this project still remains to be the segmentation of brain from the MRI slices which is nothing but the differentiation of brain and non-brain tissue in MRI (termed as brain extraction or skull stripping), and the non-linear warping of MRI images with corresponding histological slices.

Automated Image Processing Technique Flowchart The method to coregister MEmMRM to histology will consist of four independent processes as described in the following table 3.1

Table 3.1: Principle steps of the Automated Image Processing Technique

- | |
|---|
| <ol style="list-style-type: none"> 1. A brain MRI extraction technique. 2. A 3D blockface volume reconstruction. 3. A 3D linear registration of the MRI volume to the blockface volume. 4. A 2D non-linear registration (warping) of the MRI and histological slices to corresponding blockface slices. |
|---|

The co-registration process is illustrated in figure 3.1. First, using level set image segmentation method the mouse brain slices are extracted from the whole head MRI and these MRI slices are stacked in 3D to create the entire in-vivo brain volume. In the second step the blockface brain slices are segmented out from the intermediate blockface images and stacked up in 3D to reconstruct 3D blockface volume. Then MRI volume undergoes 3D registration(affine transformation) and resliced to match the orientation of the blockface volume. Finally, both histological slices and resliced MRI are warped to the blockface images using Thin Plate spline (TPS) algorithm to correct for slice specific deformations. In this process of warping (TPS algorithm) automatic scheme is developed for selection of point landmarks and also its optimization based on the maximization of Normalized Mutual information or NMI between the histological image and the warped image.

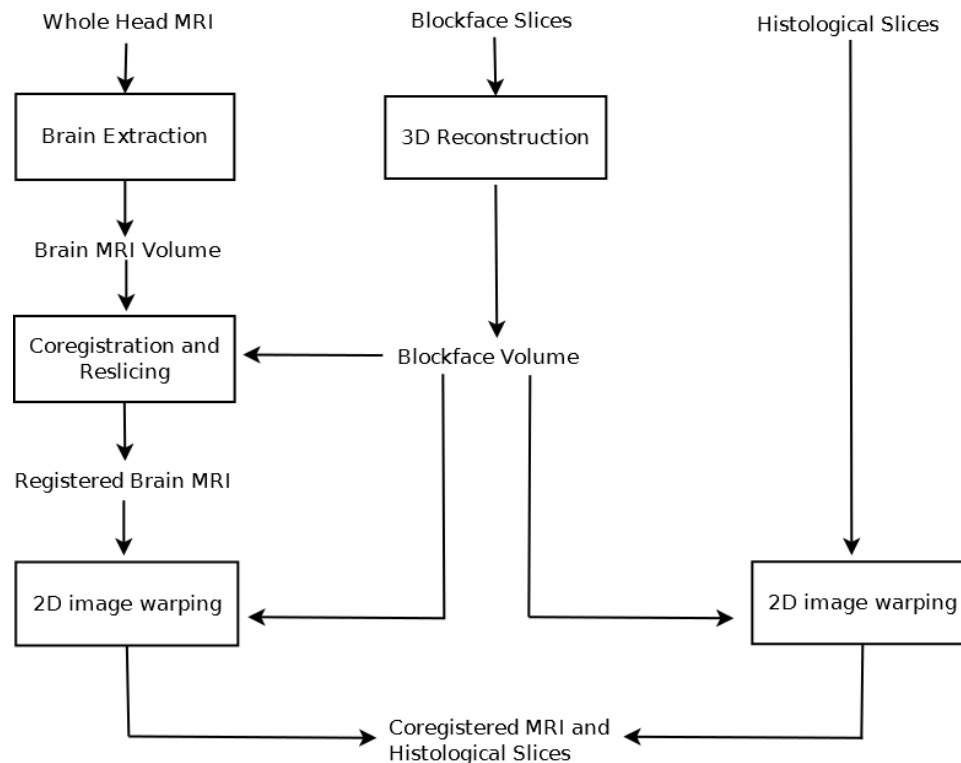


Figure 3.1: Flowchart of the MRI and histology co-registration procedure. Texts without boxes represent data; boxed texts represent data processing procedures. Arrows entering a box represent input for transformation.

3.1.1 Brain Extraction from MR images

One of the most challenging problems in this project is extracting the brain volume from whole head MRI. The differentiation of brain and non-brain tissue from MRI image and corresponding segmentation of only the brain portion is a difficult task because the pixel intensity is almost similar in both kinds of tissues and due to partial volume effect (ref) the edges are also not clearly evident. Extraction of the brain volume from whole head MRI is also known popularly as skull stripping and it is a required step for image processing and analyses including brain volume measurements, co-registration with histology, co-registration of MRI acquired at different times, and identification of brain neuro-structures. Several image

segmentation techniques have been employed for brain extraction. Level set curve evolution technique yields better results than any other technique in this aspect and it is researched extensively for this purpose. Level sets belong to broad family called active contour models. In active contour model segmentation approach an initial curve is determined inside a particular structure in the image and the curve is expanded based on energy functionals, when a balance equilibrium is attained the curve function gives the approximate boundary of the image. The curve propagation, including its speed and the accuracy of its final position, can depend on image properties, constraints on the curve, and a priori knowledge of the object. Level sets are better fit in this scenario because it results in more perfect segmentations around cusps, corners, and may break or merge naturally during the evolution, and the topological changes are thus automatically handled.

Some important points about brain extraction from MR images should be mentioned in this context. As described in the previous paragraph advanced algorithms like level sets have been applied with considerable success in brain extraction procedures. But in case of rodent brain the situation is a little more complicated. The inherent anatomy and size of mouse brain makes the brain extraction algorithm challenging. Even at considerably highest field intensity the T₁-wt MRI and PD images of the mouse brain yields brain tissues and the non-brain surrounding tissues of almost same graylevel intensities. Moreover the gap between the brain and the surrounding tissues is so narrow that the gradient at the edges are relatively small and sometimes it is even non-discernible. At several places there is almost no visible gap and it is of the order of 150 μm spatial resolution. In this case more sophisticated segmentation algorithm with level-sets incorporated with prior knowledge about the brain image is developed.

Though in these sophisticated algorithm human intervention is considerably high to incorporate the prior knowledge about the image. The following figure 3.2 give a pictorial overview of the brain extraction method that we are working on, which described in more details in section 3.2.

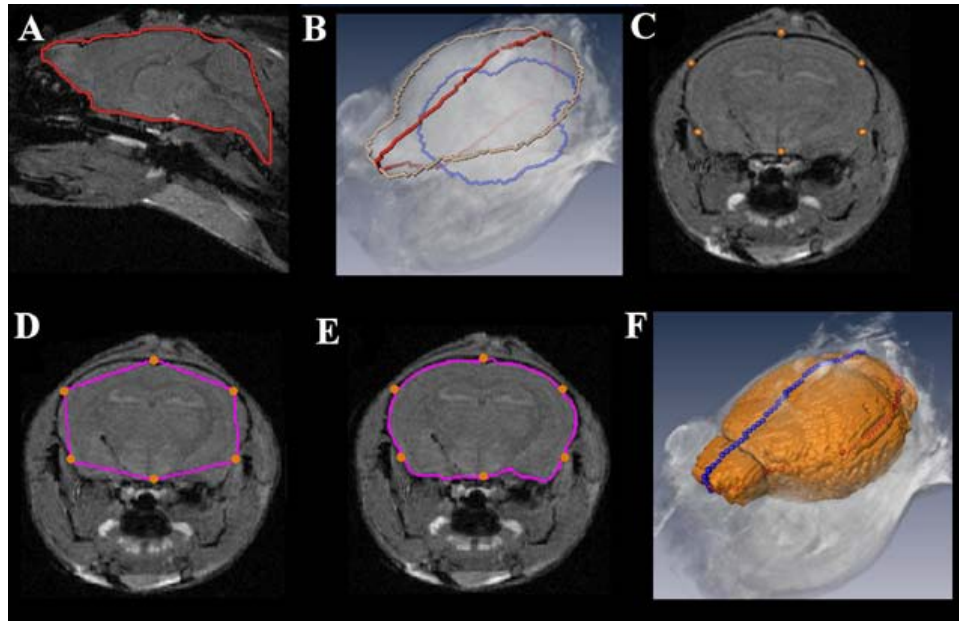


Figure 3.2: Brain extraction using a level set method. A: Selection of constrain contour on one sagittal slice and B: two axial slices. C: Constrain points defined on coronal slices from contours are D: used to automatically define a starting contour. E-F: Resulting brain extraction

3.1.2 Image Warping for Nonlinear MRI-Histology Registration

In order to reduce the global deformation between the MRI image volume and the blockface reconstructed volume and to simplify the 2D image warping, 3D image volume alignment is performed. But each histological section is subject to different distortions during slicing and handling, requiring individual 2- D slice-by-slice

warping for the registration to in vivo images. Non-linear co-registration or image warping is a method with which we try to compensate the local deformation of each MRI image slice with corresponding histological slice. Many image warping techniques have been developed including polynomial functions, B-splines, mesh warping, thin-plate splines and pseudophysical models. In this project thin-plate splines have been used for histological section warping due to the capability to correct severe distortion and computational efficiency.

Implementation of thin-plate spline registration algorithm needs to determine two sets of point landmarks specified on both source (image to be warped, e.g., histological section or MRI slice) and target (image to be registered on, e.g., blockface image) images. The landmarks are considered to be the points of one to one correspondence which are pre-determined and these landmarks will be matched exactly between the source and target images, and other part of the source image will be warped using the thin-plate splines accordingly. It is evident that the selection of landmarks is an important part of this registration procedure, the accuracy of the registration procedure depends on the correctness of landmark selection. Manual selection of point landmarks for the thin-plate splines is an error prone and time-consuming procedure. Image features were used for landmark selection in previous studies. But irrespective of how accurately the initial landmarks are chosen, it cannot be guaranteed the exact correspondence between the source and target landmarks which is the underlying assumption of thin-plate splines. In this project we develop an automatic landmark selection technique. Arbitrary set of initial landmarks are provided to the system, the landmark positions are optimized in an iterative manner maximizing the Normalized Mutual information(NMI) between the warped image and the histological slices. The following figure 3.3

gives an overview of how the non-linear co-registration process is approached, it is discussed in details in section 3.5.

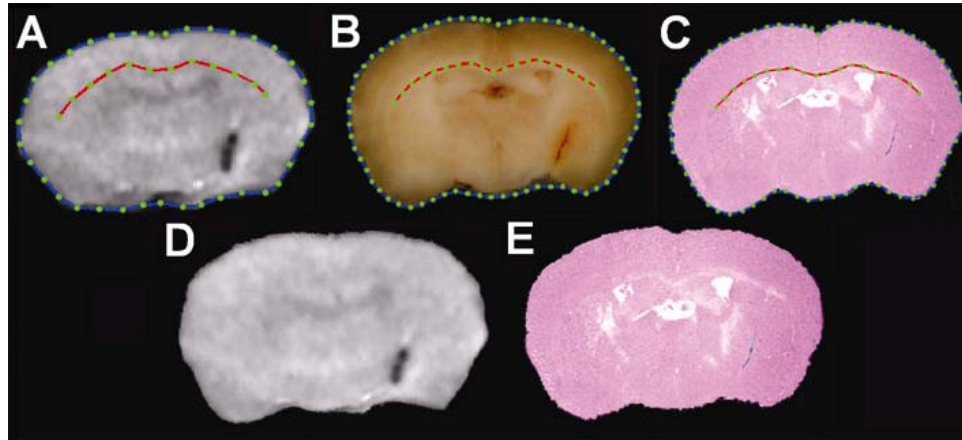


Figure 3.3: Image warping using thin-plate splines with landmark optimization. Contours of the brain boundary and corpus callosum were manually traced on the MRI (A) and histology (C) to generate landmarks. Similarly, corresponding contours on the blockface were traced to generate the homologues of the landmarks (B). (D, E): The warped MRI slice (D) and histological slice (E) using thin-plate splines. BMM clusters appear on the MRI image (black line) (A and D) and on the histological section (blue line) (C and E).

3.2 Level-Set in Brain Extraction on MRM

3.2.1 Introduction

Level set methods were first introduced by Osher and Sethian. They showed how to propagate interfaces under various constraints on the speed to obtain an entropy-satisfying solution. Most of the ideas originated from the equations used in fluid

mechanics and gas laws. Malladi, Sethian and Vemuri later showed how to use these ideas for shape modeling in images. The results obtained by implementing the technique described in are shown in this report and a detailed description of their technique is also presented. The primary advantage of this technique is that it can model complex shape features such as sharp corners. In fact, the contour can split and merge to detect multiple objects in the image. The equations are also easy to extend to higher dimensions. In implementing the traditional level set methods, it is numerically necessary to keep the evolving level set function close to a signed distance function. Reinitialization, a technique for periodically re-initializing the level set function to a signed distance function during the evolution, has been extensively used as a numerical remedy for maintaining stable curve evolution and ensuring usable results. This report discusses a new variational formulation that forces the level set function to be close to a signed distance function, and therefore completely eliminates the need of the costly re-initialization procedure and applies the concept in Medical Image Segmentation.

3.2.2 Motivation

In Medical image processing, Segmentation plays the pivotal role in determining and quantization of the position and size of various organs. In this project images of brain as obtained by Magnetic Resonance Imaging(MRI) and effective segmentation of the brain from the rest of the image is being considered. Anatomically the brain (see fig. below) is being surrounded by tissues like Duramater (consisting of Periosteal Layer and Meningeal Layer), Arachnoid mater, Pia matter, which

protects the brain, allows blood circulation to the cerebral cortex and the circulation of Cerebro-Spinal Fluid(CSF) through the Arachnoid matter(specifically sub-arachnoid space). These connective tissues around the brain are very closely attached to the brain tissues and show up with almost same intensity as the brain tissues in MRI images. The challenge and motivation of this project is the application of Level Set methods to determine the boundary of the brain with preciseness.

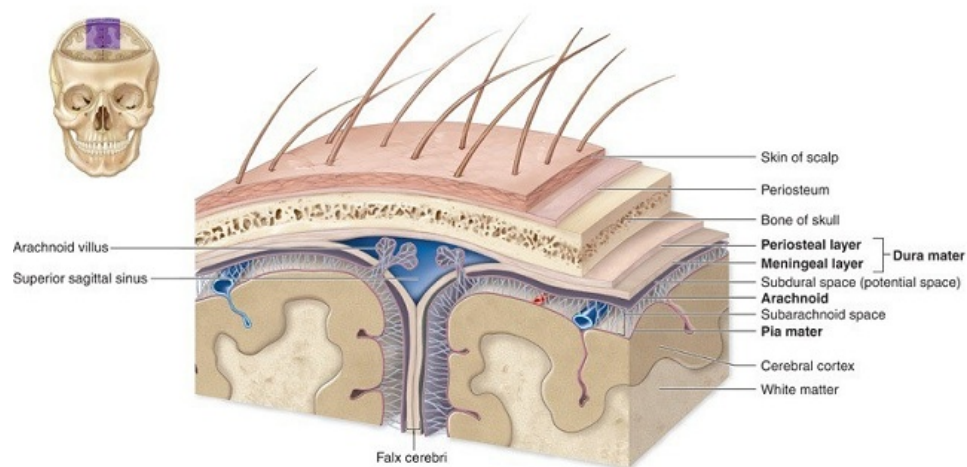


Figure 3.4: Connective tissues around the brain

3.2.3 Theory

Traditional Level Set Method In level set formulation of moving fronts (or active contours), the fronts, denoted by C , are represented by the zero level set

$$C(t) = \{(x, y) | \phi(t, x, y) = 0\} \quad (3.1)$$

of a level set function ϕ . The evolution equation of the level set function ϕ can be written in the following general form:

$$\frac{\partial \phi}{\partial t} + F|\nabla \phi| = 0 \quad (3.2)$$

which is called level set equation. The function F is called the speed function. For image segmentation, the function F depends on the image data and the level set function ϕ .

In traditional level set methods, the level set function ϕ can develop shocks, very sharp and/or flat shape during the evolution, which makes further computation highly inaccurate. To avoid these problems, a common numerical scheme is to initialize the function ϕ as a signed distance function before the evolution, and then reshape (or re-initialize) the function ϕ to be a signed distance function periodically during the evolution. Indeed, the re-initialization process is crucial and cannot be avoided in using traditional level set methods.

Algorithm of the level-set method for shape modeling

1. Calculate the image gradient at each point in the image.
2. Initialize ϕ , this is done by first making $\phi = 0$ at the points specified by the user in the initial boundary. The value of ϕ at all the other points is $\pm d_{xy}$, where d_{xy} is the distance of point (x, y) from the closest point on the level set. The value is positive or negative depending on whether the point is outside or inside the boundary.

3. Calculate the velocity at the points on the level set $\phi = 0$ using the equations given in the previous section. The velocity of other points is equal to the velocity of the closest point on the level set $\phi = 0$. This step is known as extending the velocity. This is done because, the curvature term is defined only on the front, so it does not make sense to calculate velocities at every point but it should only be calculated at the front.
4. Use the velocities to update the function using equation.
5. Repeat steps 2 through 4 till the solution converges or for a fixed (large) number of iterations.
6. The function is reinitialized every fixed number of iterations to the signed distance function. The standard re-initialization method is to solve the following reinitialization equation

$$\frac{\partial \phi}{\partial t} = \text{sign}(\phi_0)(1 - |\nabla \phi|) \quad (3.3)$$

where ϕ_0 is the function to be re-initialization, and $\text{sign}(\phi_0)$ is the sign function.

Drawbacks Associated with Re-initialization

1. Unfortunately, if ϕ_0 is not smooth or ϕ_0 is much steeper on one side of the interface than the other, the zero level set of the resulting function ϕ can be moved incorrectly from that of the original function.

2. Moreover, when the level set function is far away from a signed distance function, these methods may not be able to re-initialize the level set function to a signed distance function. In practice, the evolving level set function can deviate greatly from its value as signed distance in a small number of iteration steps, especially when the time step is not chosen small enough.

Variational Level Set Formulation of Active Contours without Re-initialization

As discussed in Chunming et.al. it is crucial to keep the evolving level set function as an approximate signed distance function during the evolution, especially in a neighborhood around the zero level set. It is well known that a signed distance function must satisfy a desirable property of $|\nabla\phi| = 1$. Conversely, any function ϕ satisfying $|\nabla\phi| = 1$ is the signed distance function plus a constant. Naturally, we propose the following integral

$$\rho(\phi) = \int_{\Omega} \frac{1}{2} (|\nabla\phi| - 1)^2 dx dy \quad (3.4)$$

as a metric to characterize how close a function ϕ is to a signed distance function in $\Omega \subset \mathbf{R}^2$. With the above defined $\rho(\phi)$, we propose the following variational formulation

$$E(\phi) = \mu\rho(\phi) + E_m(\phi) \quad (3.5)$$

where $\mu > 0$ is a parameter controlling the effect of penalizing the deviation of ϕ from a signed distance function, and $E_m(\phi)$ is a certain energy that would drive the motion of the zero level curve of ϕ . We denote by $\frac{\partial E}{\partial \phi}$, the Gateaux derivative (or

first variation) of the functional E , and the following

$$\frac{\partial \phi}{\partial t} = -\frac{\partial E}{\partial \phi} \quad (3.6)$$

is the gradient flow that minimizes the function E .

In image segmentation, active contours are dynamic curves that moves toward the object boundaries. To achieve this goal, we explicitly define an external energy that can move the zero level curve toward the object boundaries. Let I be an image, and g be the edge indicator function defined by

$$g = \frac{1}{1 + |\nabla G_\sigma * I|^2} \quad (3.7)$$

where G_σ is the Gaussian kernel with a standard deviation σ . We define an external energy for a function $\phi(x, y)$ as below

$$E_{g,\lambda,\nu}(\phi) = \lambda L_g(\phi) + \nu A_g(\phi) \quad (3.8)$$

where $\lambda > 0$ and ν are constants, and the terms $L_g(\phi)$ and $A_g(\phi)$ are defined by

$$L_g(\phi) = \int_{\Omega} g \delta(\phi) |\nabla \phi| dx dy \quad (3.9)$$

$$A_g(\phi) = \int_{\Omega} H(-\phi) dx dy \quad (3.10)$$

respectively, where δ is the univariate *Dirac function*, and H is the *Heaviside function*.

Now, we define the following as the total energy function

$$E(\phi) = \mu\rho(\phi) + E_{g,\lambda,\nu}(\phi) \quad (3.11)$$

The external energy $E_{g,\lambda,\nu}$ drives the zero level set towards the object boundaries, while the internal energy $\mu\rho(\phi)$ penalizes the deviation of ϕ from a signed distance function during its evolution. By calculus of variations, the Gateaux derivative (first variation) of the functional E can be written as

$$\frac{\partial E}{\partial \phi} = -\mu[\Delta\phi - \text{div}\left(\frac{\nabla\phi}{|\nabla\phi|}\right)] - \lambda\delta(\phi)\text{div}\left(g\frac{\nabla\phi}{|\nabla\phi|}\right) - \nu g\delta(\phi) \quad (3.12)$$

where δ is the Laplacian operator. Therefore, the function ϕ that minimizes this functional satisfies the Euler-lagrange equation

$$\frac{\partial E}{\partial \phi} = 0 \quad (3.13)$$

The steepest descent process for nomination of the functional E is the following gradient flow:

$$\frac{\partial \phi}{\partial t} = \mu[\Delta\phi - \text{div}\left(\frac{\nabla\phi}{|\nabla\phi|}\right)] + \lambda\delta(\phi)\text{div}\left(g\frac{\nabla\phi}{|\nabla\phi|}\right) + \nu g\delta(\phi) \quad (3.14)$$

The gradient flow is the evolution equation of the level set function in the proposed method.

3.2.4 Level Set segmentation

Loading an image A set of whole head MRI images was taken in the coronal plane are generated by previous procedure as described in 4.1.1. This section explains with one of the MRI slices of how the level set segmentation procedure described in chapter 3, can be applied to segment out just the brain from a whole head MRI. A MRI image of the brain which was chosen and loaded into the system.



Figure 3.5: The whole head MRI slice from which the brain is segmented

Calculation of Edge Indicator Function Let I be the image considered here. The Gaussian Kernel G_σ for $2D$ is defined as

$$G_\sigma(x, y) = \frac{1}{2\pi\sigma^2} \exp^{-\frac{x^2+y^2}{2\sigma^2}} \quad (3.15)$$

where (x, y) are the co-ordinates of a point on a $2D$ plane and σ is the standard deviation. The Image is first histogram equalised to make the image data spread out through the entire range of $0 - 255$ and the following Image shows the initial histogram and the modified histogram. This step is done to improve the contrast of the image and thus make the edges more pronounced.

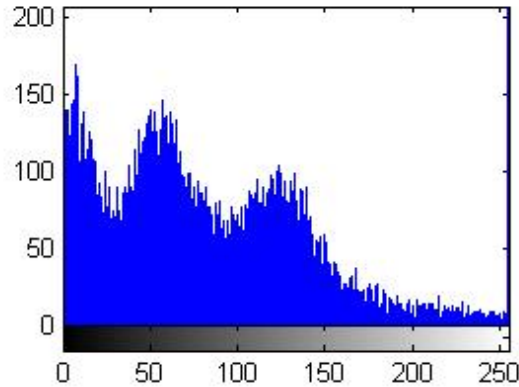


Figure 3.6: Original Histogram of the Image

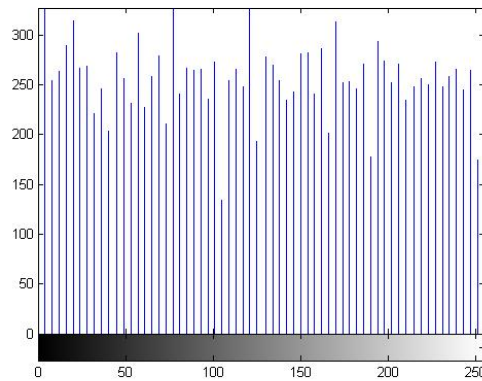


Figure 3.7: Modified Histogram of the Image

$G_\sigma * I$ can be calculated easily. In this case only a $4 * 4$ window of gaussian filter with the standard deviation($\sigma = 20$) is generated, the convolution of the Gaussian Filter with the original image I results in the following smoothed image

The corresponding edge indicator function over the image I is displayed in the figure below

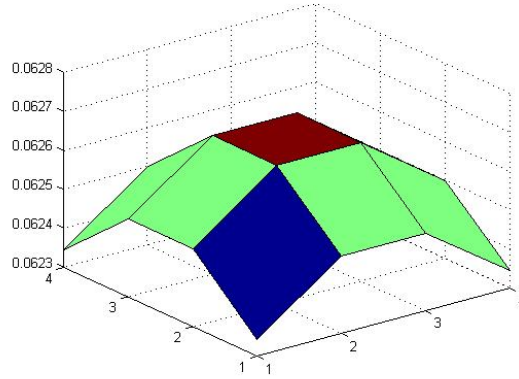


Figure 3.8: The Gaussian Smoothing Filter

Evolution function The evolution of the Level Set is being defined by the equation

$$\frac{\partial \phi}{\partial t} = \mu \left[\Delta \phi - \operatorname{div} \left(\frac{\nabla \phi}{|\nabla \phi|} \right) \right] + \lambda \delta(\phi) \operatorname{div} \left(g \frac{\nabla \phi}{|\nabla \phi|} \right) + \nu g \delta(\phi) \quad (3.16)$$

where $\delta(x)$ is the Dirac function. In practice, the Dirac function is slightly smoothed as the following function

$$\delta_\epsilon = \begin{cases} 0 & |x| = 0 \\ \frac{1}{2\epsilon} [1 + \cos(\pi x / \epsilon)] & |x| \leq \epsilon \end{cases} \quad (3.17)$$

and regularized Dirac function $\delta_\epsilon(x)$ with $\epsilon = 1.5$

Selection of time step τ In this method the time step can be chosen significantly larger than the time-step used in the traditional level set algorithm. But in order to maintain stable level-set evolution the time step τ and the coefficient μ must



Figure 3.9: The Convolution of the original Image and the Gaussian Filter satisfy

$$\tau \cdot \mu < 0.25 \quad (3.18)$$

Using larger value of τ speeds up the curve evolution but it may cause error in the boundary location if the time step is chosen too large. There is a trade-off between choosing larger time step and accuracy in boundary location. Usually, $\tau \leq 10.0$ for most images.

Flexibility in Initial Level Set Function The level set function ϕ is not required to be initialized as a signed distance function. Let the initial Level Set function be

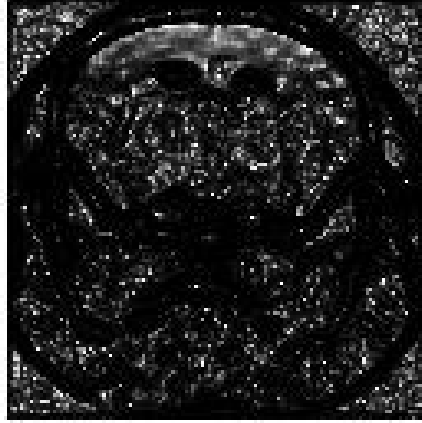


Figure 3.10: The Edge Indicator Function

$\phi_0(x, y)$ and it is defined as below

$$\phi_0(x, y) = \begin{cases} -c_0 & (x, y) \in \Omega_0 - \partial\Omega_0 \\ 0 & (x, y) \in \partial\Omega_0 \\ c_0 & (x, y) \in \Omega - \Omega_0 \end{cases} \quad (3.19)$$

where Ω_0 be a subset in the image domain Ω , and $\partial\Omega_0$ be all the points on the boundaries of Ω_0 , it is suggested to choose c_0 larger than 2ϵ , where ϵ is the width in the definition of the regularized Dirac function δ_c . In the experiment $\epsilon = 1.5$ and the value of $c_0 = 4$.

The figure 3.11 and 3.12 show how the level set curve and the corresponding contour grows with increasing iterations. The figure ?? is the initial image that we

started with and the final segmented image that we get after applying Level Set Evolution algorithm is shown in 3.13.

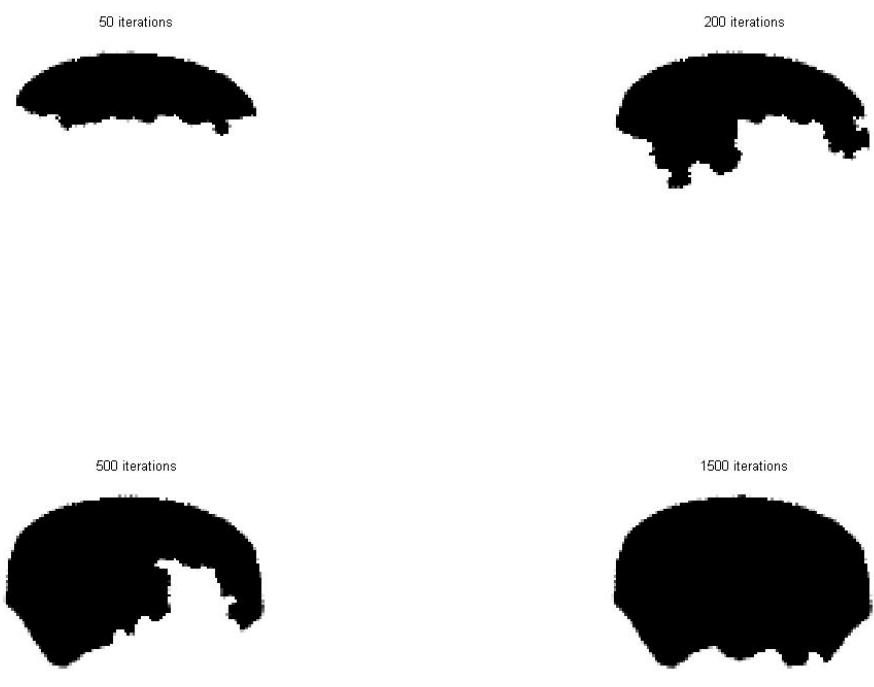


Figure 3.11: The Evolution of Level Set Function: (a) after 50 iterations (b) after 200 iterations (c) after 500 iterations (d) after 1500 iterations

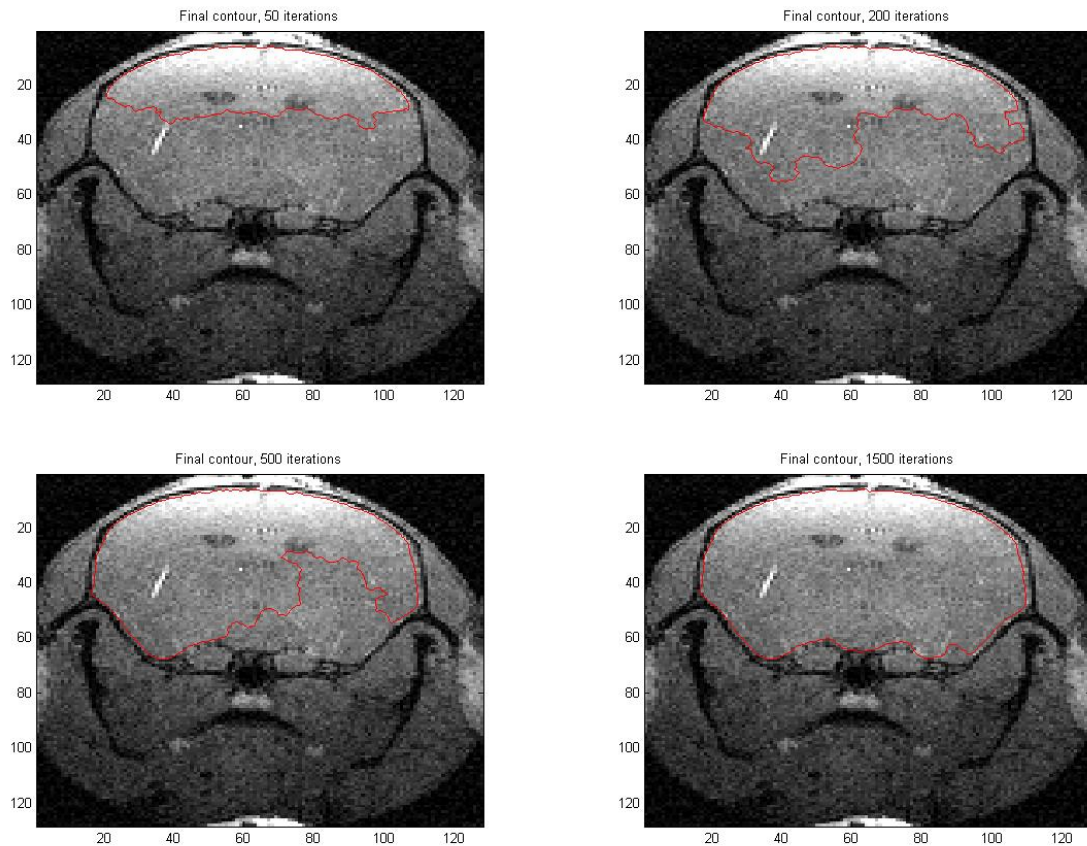


Figure 3.12: The Evolution of Level Set Contour: (a) after 50 iterations (b) after 200 iterations (c) after 500 iterations (d) after 1500 iterations

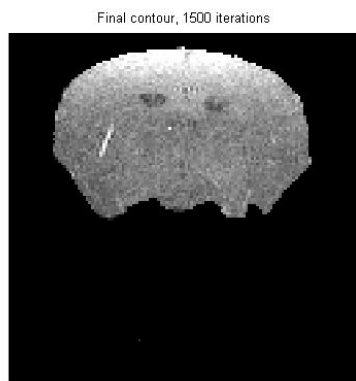


Figure 3.13: The Final Segmented Image of the Brain from the initial image

The brain segmentation from the entire MRI volume (also known as skull stripping) can be approached in a different way. Instead of applying Level Set segmentation approach on 2D brain slices and stacking them up to create 3D volume, the Level Set algorithm can be modified to be applied in 3D nifty volume directly to segment the brain volume as a whole. The biggest disadvantage of this procedure is that the brain intensity and topological characteristics are varying in different regions of the volume and hence the parameters which are set for the preprocessing as well as edge indicator functions will need to be changed accordingly. As a solution to this problem the entire volume is divided into subvolumes such as brain₁, brain₂, brain₃ etc. This method is exactly similar to the way the blockface images were generated of the sub-volumes, not the entire brain taken as a whole (described in details in Section 3.3). Each of the sub-volumes consists of 20-25 coronal slices of the rat brain on an average. On successful determination of volume with 3D levelset methods the sub-volumes are arranged in order to create the entire brain volume. It is assumed that the image characteristics of the 20-25 adjacent coronal slices are very similar. In the exact fashion of determination of 2D levelset segmentation, the initial volume is placed interactively by the user in the volume of interest and the curve is let to evolve and gradually we get the segmented brain volume. The figure 3.21 shows some steps in the 3 D curve evolution and the corresponding volume generated.

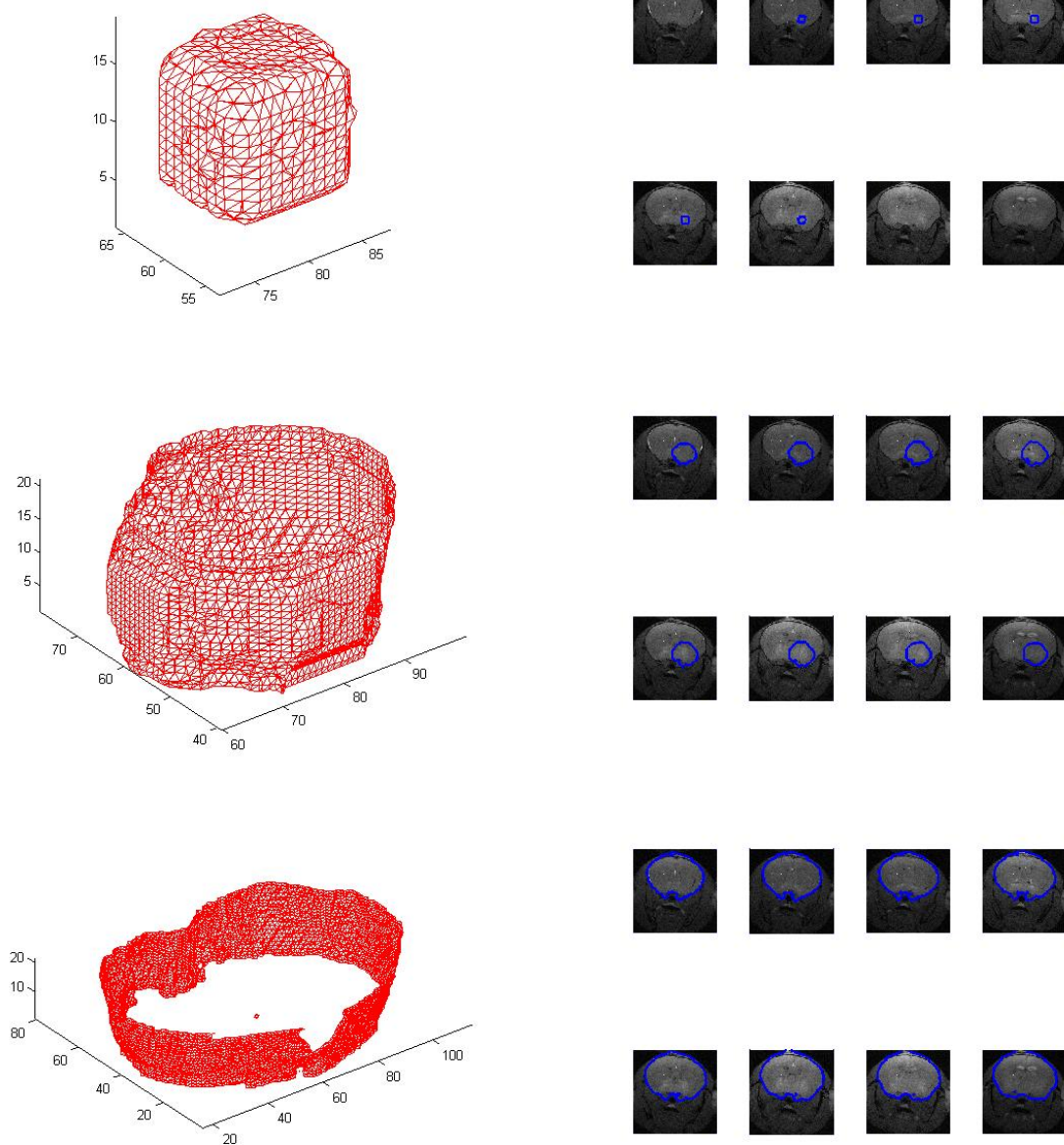


Figure 3.14: The Evolution of 3D Level Set volume curve: (a) after 1 iteration (b) after 15 iterations (c) after 80 iterations

3.3 Blockface Image Segmentation

This section defines about how the blockface images are generated and the image segmentation techniques applied on these images. The rat brain is physically taken out of the cranium and fixed in paraffin. After this step is done the entire brain is sliced in the coronal plane at an interval of $150 \mu m$. Pictures of each of these slices are the blockface images. We have used histogram equalization, Gaussian smoothing and canny edge detection principle to segment the brain slices from the actual blockface slices. Here we briefly discuss the theoretical concepts of the techniques used and how the approach to our problem was designed based on these concepts.

3.3.1 Histogram Equalization

Histogram equalization is considered as a very popular and extensively used image pre-processing tool that is used for improving the contrast of the image under consideration. It is mostly found that in the medical images the edges are not properly defined and they are pretty blurred; in that case the image enhancement techniques need to be used for getting a better understanding of the image and also as a pre-processing step for other algorithms to be applied. It is commonly found that the pixel values in an image only cover a certain part of the entire gray-level values. The idea of Histogram equalization is to distribute the intensity values across the entire gray-level and thus it enhances the contrast. In a grayscale

image, Probability Density Function of an image is defined as average number of pixels per gray-scale value. Mathematically it can be expressed as

$$p_x(i) = p(x = i) = \frac{n_i}{n}, 0 \leq i < L \quad (3.20)$$

where L is the total number of gray levels in the image, n is the total number of pixels in the image and n_i is the number of pixels in graylevel i .

The cumulative distribution function is the summation of all the graylevel pixels below a certain graylevel in the image. It can be expressed as

$$cdf_y(i) = \sum_{j=0}^i p_x(j) \quad (3.21)$$

Histogram equalization is a linear mapping of the cumulative distribution function to make the graylevel values stretch through the entire grayscale. The mapping can be defined as

$$y = T(x) = cdf_x(x) \quad (3.22)$$

$$y' = y \cdot (\max\{x\} - \min\{x\}) + \min\{x\} \quad (3.23)$$

3.3.2 Canny Edge Detector

The Canny edge detector algorithm is a very popular edge detection principle coined by John Canny (ref). In this problem the edge detection problem is modeled as a signal processing optimization problem. The solution to edge determination problem is actually a rather complex exponential function, but canny edge detection follows several ways to approximate and optimize the edge-searching problem. The following are the important steps involved in canny edge detection algorithm

1. As a part of pre-processing the image is smoothed by convolution with a 2D Gaussian filter. In order to reduce the computational complexity instead of using a 2D Gaussian 2 one dimensional Gaussian filters can be used in each dimension of the image.(ref)
2. The gradient of the image determines the relative difference in the values of neighboring pixels. Therefore the positions of abrupt change in the gradient determine the places of higher intensity changes, which show the presence of edges in those regions.
3. The gradient calculated in the previous step should be maximum at the edges because the maximum intensity change between 2 adjacent pixels are at the edges. Hence the gradient at each pixel is calculated and then it is compared with the gradients of all other pixels in the image. If it not the maximum it is neglected to be an edge point. This process is called non-maximal suppression.
4. After the potential edge points are determined, not all maximum gradient

points determine the object boundaries which are of prime importance in this case. In order to solve this problem canny edge detector uses two different threshold values, one High threshold and the other Low threshold depending on prior knowledge of the original image. Any edge point having intensities within this window of threshold values are considered to be the required edge in the image. This process of thresholding is also referred to as "hysteresis".(ref)

3.3.3 Blockface Image Segmentation

Loading an image A set of blockface images taken in the coronal plane are generated by previous procedure as described in the subsection4.1.2. This section explains with one of the Blockface Image slices of how some segmentation procedures can be applied to segment out just the brain from the entire blockface Image. We are considering only the edge of the blockface slice because that is enough information to generate the Blockface volume. A Blockface image slice of the brain which is chosen and loaded into the system.

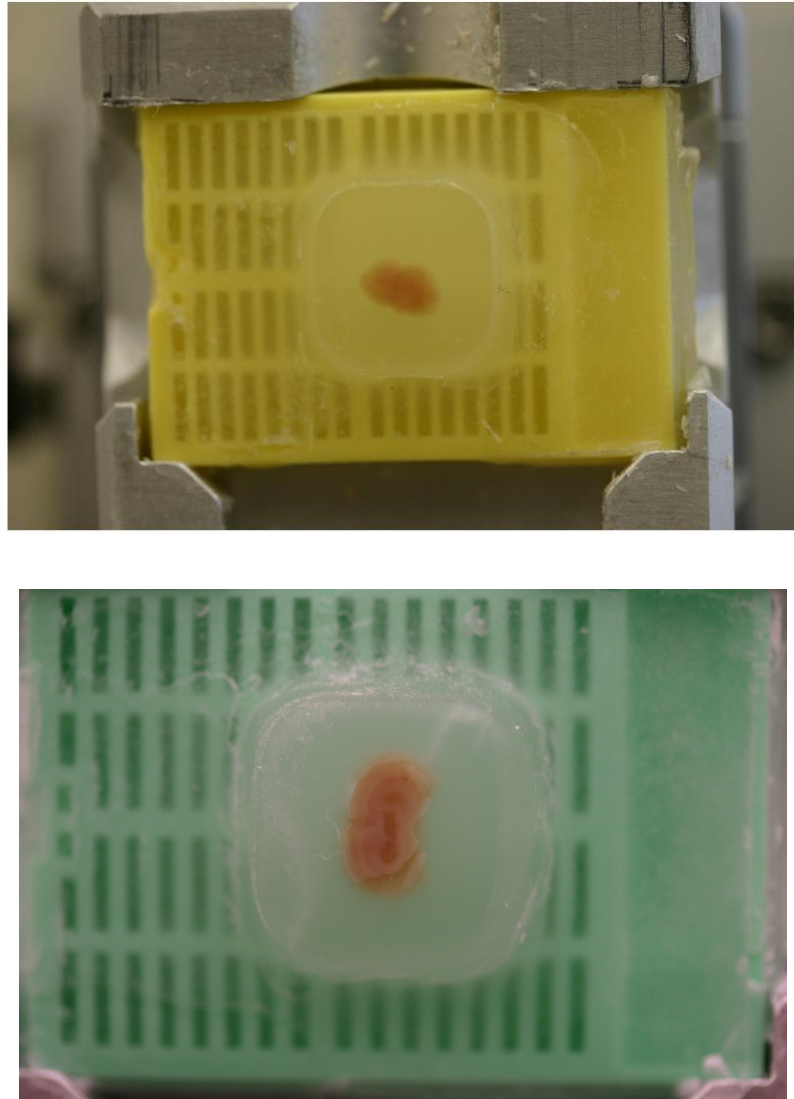


Figure 3.15: Blockface Image of the brain fixed in paraffin

As seen in figure 3.15, it contains a lot of redundant informations which is useless in segmentation and generation of the 3D blockface volume. The image was cropped to concentrate in our particular region of interest(ROI).

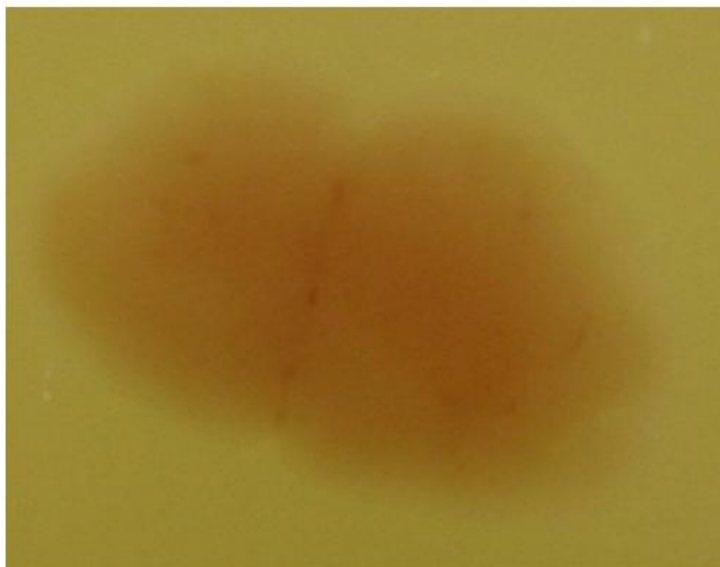


Figure 3.16: Region of Interest in the Blockface Image slice

The image thus obtained is histogram equalized to improve the contrast and thus making the edges more pronounced. A 15×15 gaussian filter is defined with a standard deviation of $\sigma = 1.5$ and the original image is convolved with the Gaussian kernel to produce a smoothed image. The following figures 3.17 and 3.18 show the Gaussian kernel used and the corresponding edge-indicator function thus produced.

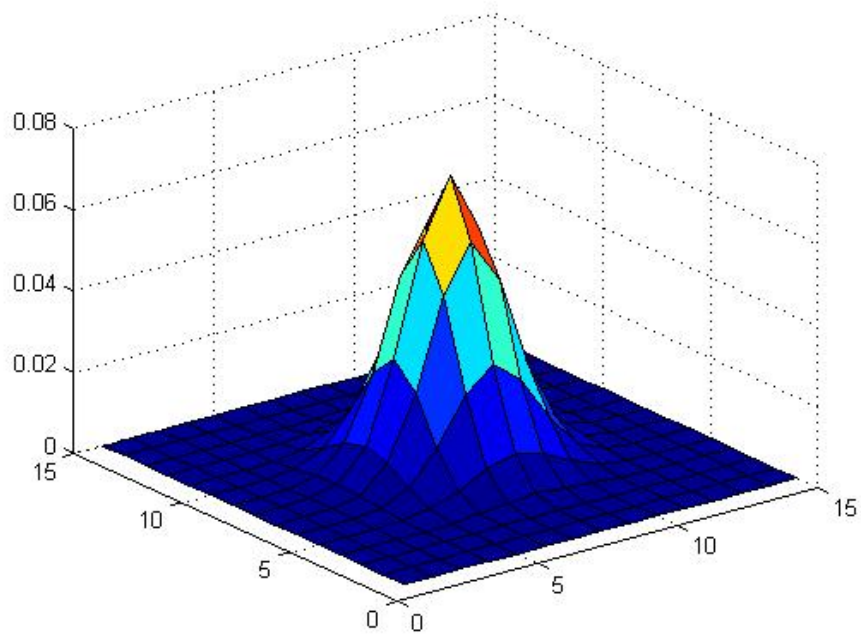


Figure 3.17: Gaussian Kernel

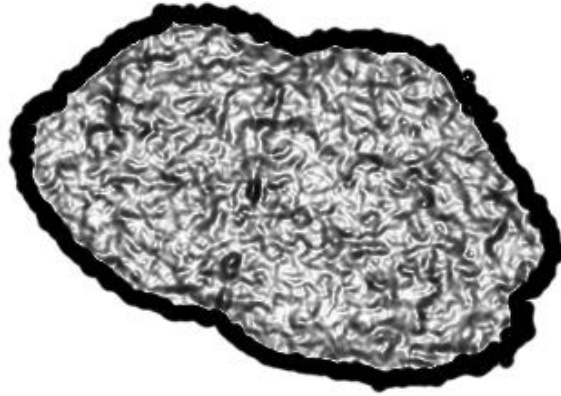


Figure 3.18: Edge Indicator function used in segmenting the blockface image

The most popular 'canny edge detection' principle is applied on the edge indicator function after the image is converted into boolean Black and White datatype thresholded at 42% of its entire gray value range. The Edge of the image thus obtained undergoes affine transformation. This Affine transformation(translation and rotation) is applied to gain alignment within each slice of the entire stack of blockface image, thus reducing the effect of mechanical shear while physically slicing the brain fixed in paraffin with the precise slicing tool at an interval of $150\mu m$. The centroid of the brain is calculated and translated to the center of the image slice as described in the figure 3.19. The orientation of the blockface brain about the principal axis is studied which gives us an estimate of the angle of tilt of the brain image and thus we rotate the image counterclockwise

to nullify the tilt. The following figure 3.19 show the affine transformation of the image and final segmented image with the centroid pointed out is showed in the figure 3.20.

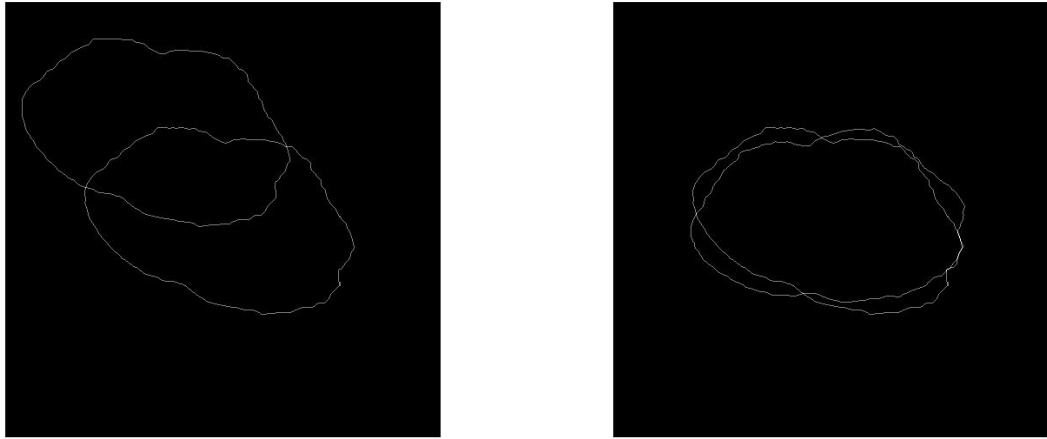


Figure 3.19: Affine Transformation of the blockface image slices: (a) Translation (b)

Rotation

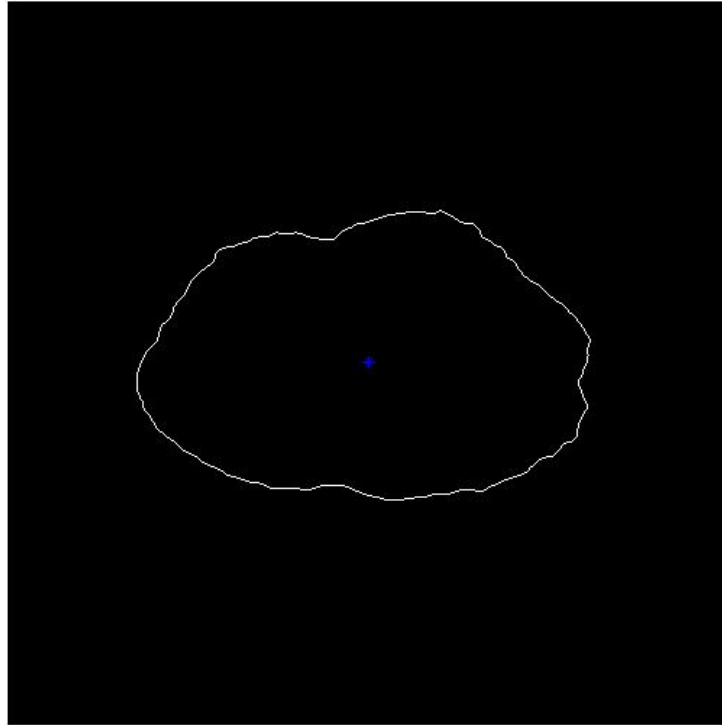


Figure 3.20: Final Segmented image of the blockface Images

The segmentation of the blockface images can be extended to include the grayscale segmentation part of the original image. In this step not only the blockface images are segmented but also the grayscale intensities of the segmented regions are restored from the original blockface images. This step is included because it is critical for the proper functioning of the next step of alignment (described in Section 3.4). The reason of the improper functioning of the volume alignment section is that affine transformation between a volume of binary images(blockface volume) and another volume of grayscale images(MRI volume) is very

difficult and may come out erroneous. The figure 3.3.3 shows some slices where the grayscale segmentation is also included. The blockface volume is generated by stacking up these segmented images in 3D. But a mapping or interpolation scheme is applied in this case. One of the very important characteristics of the blockface slices created is the thickness of the slices. This parameter should be considered when the blockface volume is recreated. Depending on the thickness of the blockface slices, image slices were replicated in adjacent volume slices to replicate the concept of interpolation.

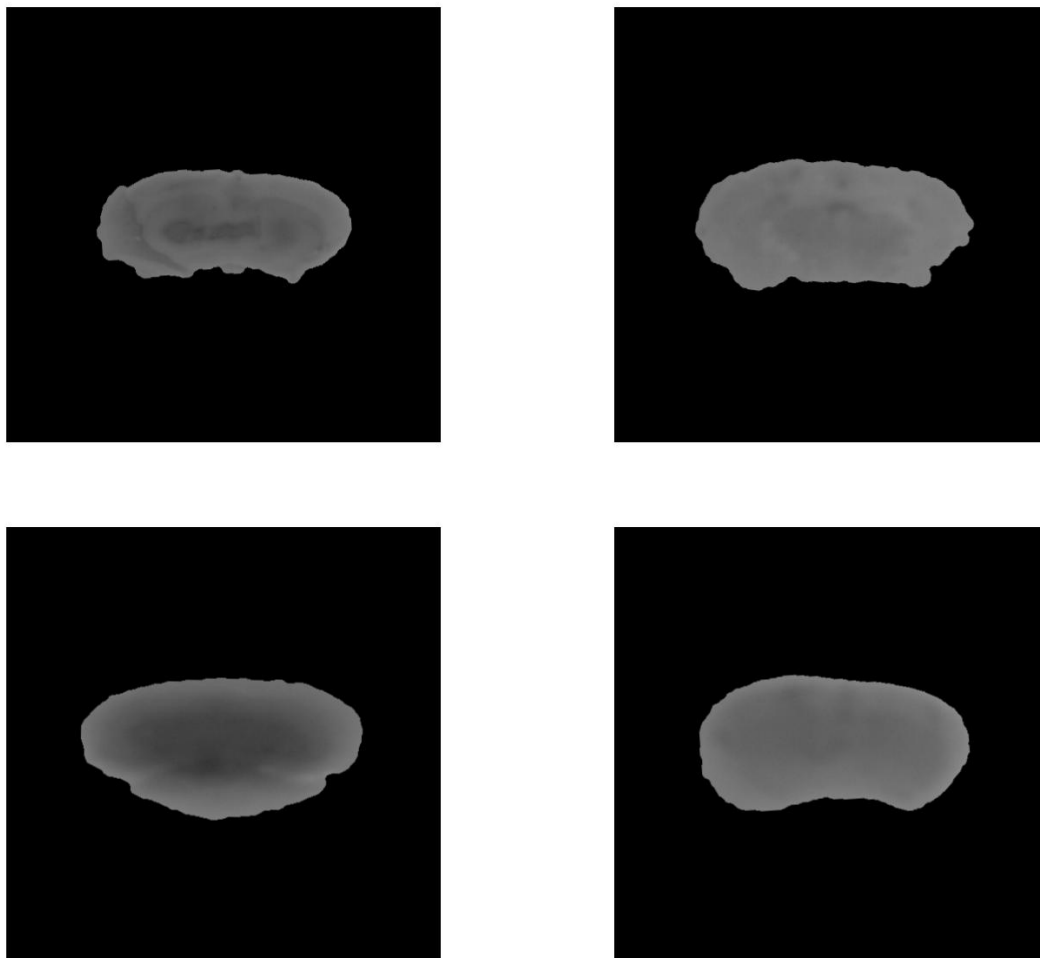


Figure 3.21: The Blockface segmented image slices where the graylevel values of the original images are also restored

3.4 Alignment

At this point of the project we only have several sets of brain MRI slices and the corresponding blockface image slices of the same brain. Though our final goal is to get the co-registration of the MRI slices and the histological images, we target to minimize the global deformations between these two sets of images. In order to do that we use the concept of 3D volume alignment of the MRI image volume and the blockface image volume. We concentrate only on affine transformation (translation and rotation in 3D) of these two image volumes. In order to achieve this alignment we use the concept of 3D registration known as demon registration as introduced by Thirion. The following paragraphs describe the driving principle behind the classical algorithm and then how it is modified to put it to our use.

In traditional demon registration principle, like other image registration algorithms, one to one correspondence between two images is determined, only difference is that the registration is in 3D and the images are 3D volume images. But it still has a static image F and another moving image M and the moving image is modified to match in orientation as the static image. Several energy functionals act as internal or external forces when one image volume is co-registered with the other one. The optical flow equation for finding small deformations in temporal image sequences is used as basis of the demon registration forces (ref). Consider a given point p in the static image F and the corresponding point of match in the moving image M be given by p' . Let the intensity of point p be f and that of p' be m . Thirion estimated the approximate displacement (velocity) u required for point p to match p' and it is given by

$$U = \frac{(m - f)\nabla f}{|\nabla f|^2 + (m - f)^2} \quad (3.24)$$

where $u = (u_x, u_y)$ in 2D, and ∇f is the gradient of the static image. Similarly like other registration algorithms there are two forces determining the registered shape of the moving image. There is an internal edge based force ∇f and the external force is $(m - f)$. In order to stabilize the velocity equation and to make the equation fit for registration, the term $(m - f)^2$ is added by Thirion. This registration method is very similar to viscous fluid model registration principles (ref). The velocity equation is modified by He Wang et. al. (ref) and he introduced another term to improve the overall edge forces and thus results in a better registration process. The modified velocity equation is shown below

$$U = \frac{(m - f)\nabla f}{|\nabla f|^2 + \alpha^2(m - f)^2} + \frac{(m - f)\nabla m}{|\nabla m|^2 + \alpha^2(m - f)^2} \quad (3.25)$$

Cachier et.al.(ref) proposed the term α as a normalizing factor which gives a balance between the two force terms.

One of the prime disadvantages of traditional demon registration algorithm is that it is inapplicable to multimodal MRI images. So a modification of the algorithm is done to make it suitable for this process. The modification in this case is known as the process of modality transformation. We utilize the concept of mutual information between two sets of images for modality transformation. Mutual information is the index of similarity in information content between 2 sets of images. The mutual information of moving image M and static image F is

defined as (ref)

$$I(M, F) = \sum_{M, F} p(m, f) \log\left(\frac{p(m, f)}{p(m)p(f)}\right) \quad (3.26)$$

where $p(m)$ and $p(f)$ are the probability distribution functions of image M and F respectively, $p(m, f)$ is the joint probability distribution derived from joint histogram approach. The proposed method uses joint histogram peaks to transform one image representation to another. In our application we are using the demon registration method for 3D alignment of MRI image volume and blockface volume. The key point to be noted in this respect is the objective behind this transformation. The global deformation parameters are tried to be reduced in this step, so the intrinsic grayscale characteristics of the MRI and Blockface images can be neglected while doing this 3D registration. The local transformation characteristics are later defined when the Thin Plate spline 2D warping is considered. Hence we represent both the MRI volume and the blockface volume as binary BLOB, that is pixels having information about the brain are considered as '1' and the rest of the 3D points are considered as '0'. Then we utilize the multimodal variant of demon registration algorithm to find the 3D aligned binary BLOB. Accordingly we can align the MRI images to match the binary BLOB. Then the MRI image volume is re-sliced to match the slicing done for histological sections and in this way we prepare the input for the non-linear co-registration system which uses Thin Plate Spline algorithm to model the local distortions.

3.5 Registration approach and Optimization

In this project we use Thin Plate Spline Warping to co-register the MRI slices and corresponding histological slices. The following sections deal briefly with the background theory of the warping method and then discuss the registration approach used in this method.

3.5.1 Thin Plate Spline Warping

Thin plate splines (TPS) were introduced to geometric design by Duchon (Duchon, 1976). The name thin plate spline refers to a physical analogy involving the bending of a thin sheet of metal. In the physical setting, the deflection is in the direction, orthogonal to the plane. In order to apply this idea to the problem of coordinate transformation, one interprets the lifting of the plate as a displacement of the or coordinates within the plane. In 2D cases, given a set of K corresponding points, the TPS warp is described by $2(K + 3)$ parameters which include 6 global affine motion parameters and coefficients for correspondences of the control points. These parameters are computed by solving a linear system.

Radial Basis Function Given a set of control points $w_i, i = 1, 2, \dots, K$, a radial basis function is a spatial mapping function which maps any location x in space to a new location $f(x)$ represented by

$$f(x) = \sum_{i=1}^K c_i \varphi(\|x - w_i\|) \quad (3.27)$$

where $\|\cdot\|$ denotes the usual Euclidean norm and c_i is a set of mapping coefficients. One possible choice for the kernel function φ is the thin plate spline $\varphi(r) = r^2 \log r$. It has a more global nature than the Gaussian kernel $\varphi(r) = \exp(-\frac{r^2}{\sigma^2})$, which is another common function, a small perturbation of one of the control points always affects the coefficients corresponding to all the other points as well. Note that a thin plate spline is generally understood as a function minimizing the integral of the squared second derivative, typically in two dimensions. This corresponds to the radial basis kernel. Other choices of radial basis kernel produce interpolation that would not normally be described as a thin plate spline. The TPS fits a mapping function $f(x)$ between corresponding point-sets y_i and x_i by minimizing the following energy function:

$$E = \int \int [(\frac{\partial^2 f}{\partial x^2})^2 + 2(\frac{\partial^2 f}{\partial xy})^2 + (\frac{\partial^2 f}{\partial y^2})^2] dx dy \quad (3.28)$$

And for a smoothing TPS, it is

$$E_{tps} = \sum_{i=1}^K (\|y_i - f(x_i)\|)^2 + \lambda \int \int [(\frac{\partial^2 f}{\partial x^2})^2 + 2(\frac{\partial^2 f}{\partial xy})^2 + (\frac{\partial^2 f}{\partial y^2})^2] dx dy \quad (3.29)$$

Then smoothing TPS is defined as

$$f_{tps} = \operatorname{argmin} E_{tps} \quad (3.30)$$

3.5.2 Automation of Landmark Selection, Registration and Optimization

Image warping is used to register mMRM and histological sections to blockface imaging. The image warping technique is developed based on thin-plate splines with point-landmark optimization. The technique developed in this project is an extension of our landmark optimization method, in which contours are manually drawn on the anatomical features on the MRI and histological sections, and corresponding landmarks are extracted from the contours and optimized according to their distance and local curvature. In this project, we fully automate the semi-automatic method with the introduction of normalized mutual information (NMI).

Implemented Technique The source image (MRI slice) will be first aligned with the target (blockface image) images using affine transformation. The edge maps (gradients) of the images will be calculated. One point landmark is placed on the centroid, and four landmarks are placed on the brain boundaries detected on

the edge maps. The four boundary landmarks are distributed every 90° from the centroid of each slice after affine transformation. The landmarks on the source image are then relaxed to move in a region A. Nonlinear transformation will be performed on the source image and the NMI of the source and target will be calculated. The source landmarks will be optimized by minimizing the cost function defined by:

$$M = \lambda * NMI(S, T) + \sum_{j=1}^n (|P_{S,j} - P_{S,j}^0|) \quad (3.31)$$

where S and T are the source and target images, respectively; n is the number of landmarks, and P_s is a point landmark; superscript "o" indicates the initial landmark location; λ is the weighting between NMI (term 1) and landmark displacement (term 2). More landmarks will added on locations of maximal gradients on the source image, and on the same locations on the target image until the pre-defined landmark number N. After adding each landmark, all source landmarks will be optimized by minimizing eqn (1). The same process will be used to warp the stained histological slices to the corresponding blockface slice(s). The landmark selection procedure is illustrated using pseudocode in Table 3.2.

The actual process of non-linear registration as described in the pseudocode of Table 3.2 can be best understood if the intermediate images and the corresponding landmarks are studied. The following figures present a pictorial representation of the landmark selection procedure and optimization of the landmarks. We have selected only one pair of MRI-histo slices and have shown the

1. Align the source image with the target image using affine transformation.
2. The brain boundary in the MRI and the histological sections are detected using 'Canny Edge Detection' principle.
3. Initial set of landmarks are specified by determining the centroid and the four boundary points distributed every 90° from the centroid of each slice.
4. Thin-plate splines are used to coregister the MRI and the histological section by warping the MRI.
5. Normalized Mutual information(NMI) of the warped MRI and the histological section is calculated.
6. For $i = 5$ to N
 - Relax source landmarks
 - Optimize source landmarks by minimizing Equation 3.31
7. End
8. More landmarks are added by sampling the brain boundary obtained from the edge detection principle described in step 2. The process goes back to step 5 to optimize the landmarks. This process of adding more landmarks is done by reducing the sampling interval along the brain boundary and is repeated until the maximum number of pre-determined landmarks, N is reached or the displacement of landmarks after optimization is lower than a pre-determined threshold or NMI between the source and target images reaches a pre-determined value.

Table 3.2: Pseudocode of the algorithm for MRI-histological slice registration

intermediate images obtained while doing the Thin Plate Spline registration procedure. Figure 3.22 shows the initial pair of MRI and histological slices before any preprocessing.

The pre-processing operation is done on both the MRI and histological slices which includes the affine transformation of both so that they are aligned with

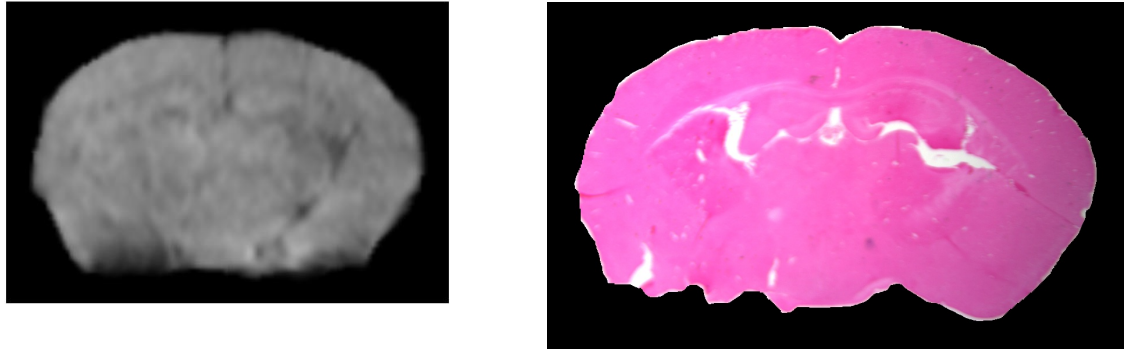


Figure 3.22: MRI histological pair of images to be registered: (a) Low resolution T₁-wt MR image (b) High resolution stained Histological image

each other. Then both the images are converted into logical BW images for further processing. The BW images are shown in Figure 3.23



Figure 3.23: (a) Logical BW representation of T₁-wt MR image (b) Logical BW representation of histological image

Canny edge detection principle is applied on the BW images on the previous step to do the gradient calculations and find out the edges. The edge detection is a critical process because the landmarks selected on the images for Thin plate spline algorithm are going to be placed on the edges; the corresponding edge of the MRI and the histological slices are shown in the Figure 3.24.

Once the edges are determined an arbitrary set of landmarks are decided.

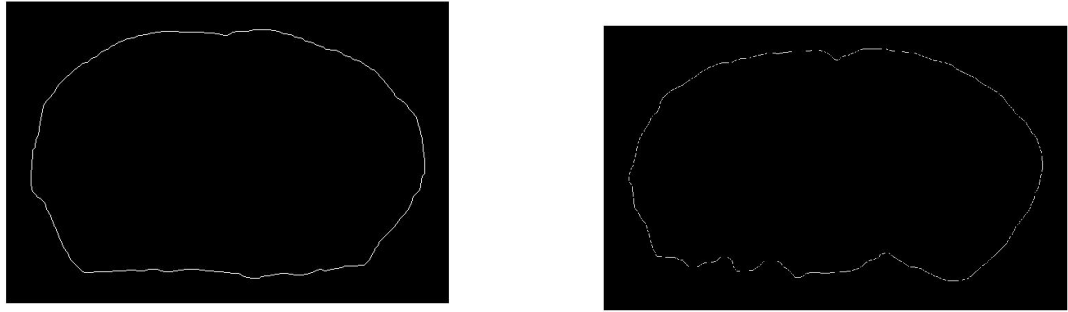


Figure 3.24: (a) Canny Edge detection of T₁-wt MR image (b) Canny Edge detection of histological image

As an arbitrary choice the centroid and four boundary points on the edge distributed every 90° are chosen as initial landmarks. Figure 3.25 shows the initial arbitrary landmarks pointed on both the images.

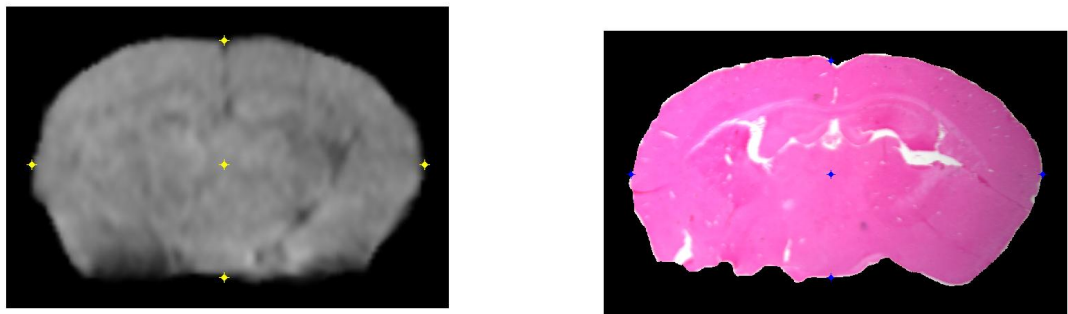


Figure 3.25: (a) Initial 5 landmarks determined on T₁-wt MR image (b) Initial 5 landmarks determined on histological image

The optimization of the landmarks are continued iteratively, new landmarks are added by sampling the brain boundary obtained from the edge detection principle. This process of adding more landmarks is done by reducing the sampling interval along the brain boundary and is repeated until the maximum number of pre-determined landmarks, N is reached or the displacement of landmarks after optimization is lower than a pre-determined threshold or NMI between the

source and target images reaches a pre-determined value. Figure 3.26 shows the final warped image having a NMI index of 0.69. Figure 3.27 shows initial set of landmarks(yellow) and the optimized set of landmarks(blue) plotted on the same image to show the effect of landmark optimization technique used. Figure 3.28 is a superimposition of warped image and the actual histological image, it gives a sense how closely related are the two image and the perfection of the automatic landmarking and registering process used.

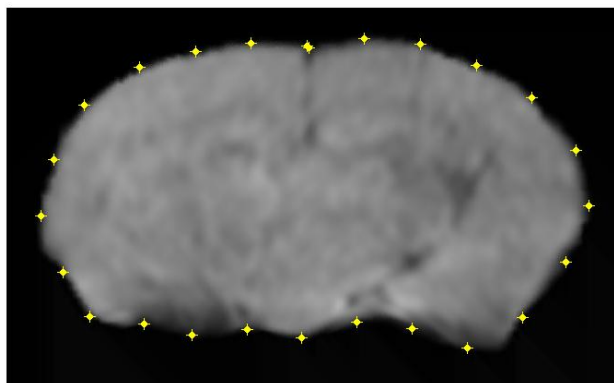


Figure 3.26: Final Warped image after the co-registration is completed. NMI index is 0.69

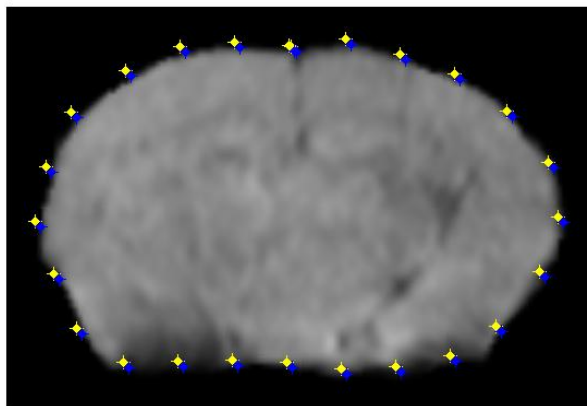


Figure 3.27: The initial landmark set(yellow) and optimized landmark set(blue)

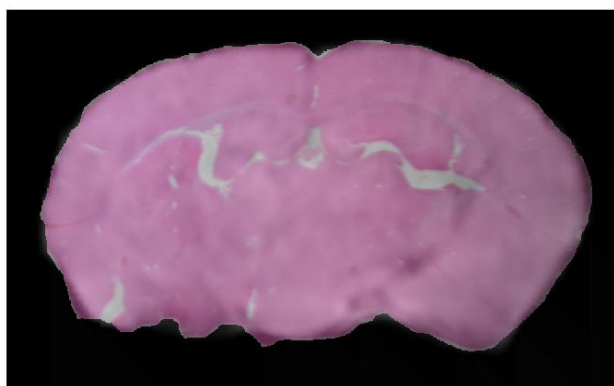


Figure 3.28: Visible similarity between the warped and histological image observed from the superimposition of the 2 images

Chapter 4

Results and Evaluations

The problem of automated landmark selection and non-linear registration of MRI images and Histological brain slices are of immense importance because of its widespread application. MRI is a non-invasive process that means the subject of concern does not need to be operated while doing the MRI. On the other hand process of making histological slides is invasive that is the concerned tissue is separated from the subject's body, stained properly and examined under the microscope. Thus our project deals with the bridge between the invasive and non-invasive methods of examining the same tissue. As we know cancer detection of a particular tissue is done by the method of Biopsy. A biopsy is a procedure to remove a piece of tissue or a sample of cells from the subject's body so that it

can be analyzed in a laboratory after making histological slides of the concerned tissues. Thus with further research in this field and incorporation of machine learning algorithms, we can design some non-invasive efficient techniques which can predict the structure of the underlying tissues.

As a part of the procedure the experimentation is done on infected rat brain. Rats are being cultured and infected with HIV-1. After the 2-3 weeks when the neuro-cognitive disorders become pronounced in the animals under experimentation then axial T2* MRI of the rat brain is performed. After the MRI was performed, brains were removed, embedded, sectioned and digital images were acquired every $150\mu m$ (blockface imaging) during sectioning within a cryostat. The same brain slices that were photographed as blockface images were then stained with Prussian blue and counterstained with hematoxylin. Ten pairs of such MRI slices and the corresponding histological slides were prepared. These ten sets of pictures are the inputs to our Automated landmark detection and Thin Plate Spline warping system. The problem that we deal in this project is to find a one-one correspondence between these two pairs of MRI and histological images in these ten different sets. Our system should be able to automatically determine an efficient set of landmark in the MRI image so that it can be effectively warped onto the histological image using non linear registration. In some semi-automatic method for landmark detection contours are manually drawn on the anatomical features on the MRI and the histological sections, and corresponding landmarks are extracted from the contours and optimized according to their distances and local curvatures. We will focus on fully automating this process with the introduction of the concept of Normalized Mutual Information, which is a widely used as a measure of image similarity. Thus the output of the system would be an automatically landmarked

MRI image which is co-registered with the corresponding histological image. This chapter describes the dataset we are working on and then describe the experimental results and corresponding evaluations.

4.1 DataSets

4.1.1 MRI slices

The MRI images considered in this experiment are obtained from the Bruker 7T scanner. The entire MRI image volume is stored in Analyze75 format. The volume is loaded into the system by MRICro software. The figure 4.1 shows how the MRI looks when it is loaded into the software. The figure 4.1(a) shows the coronal view of the rat brain which is actually one slice of the brain MRI taken from the front to back direction. In this experiment we consider only the coronal view of the MRI. So we can use the MRICro software to save only the coronal view of the MRI volume into 176 different slices.

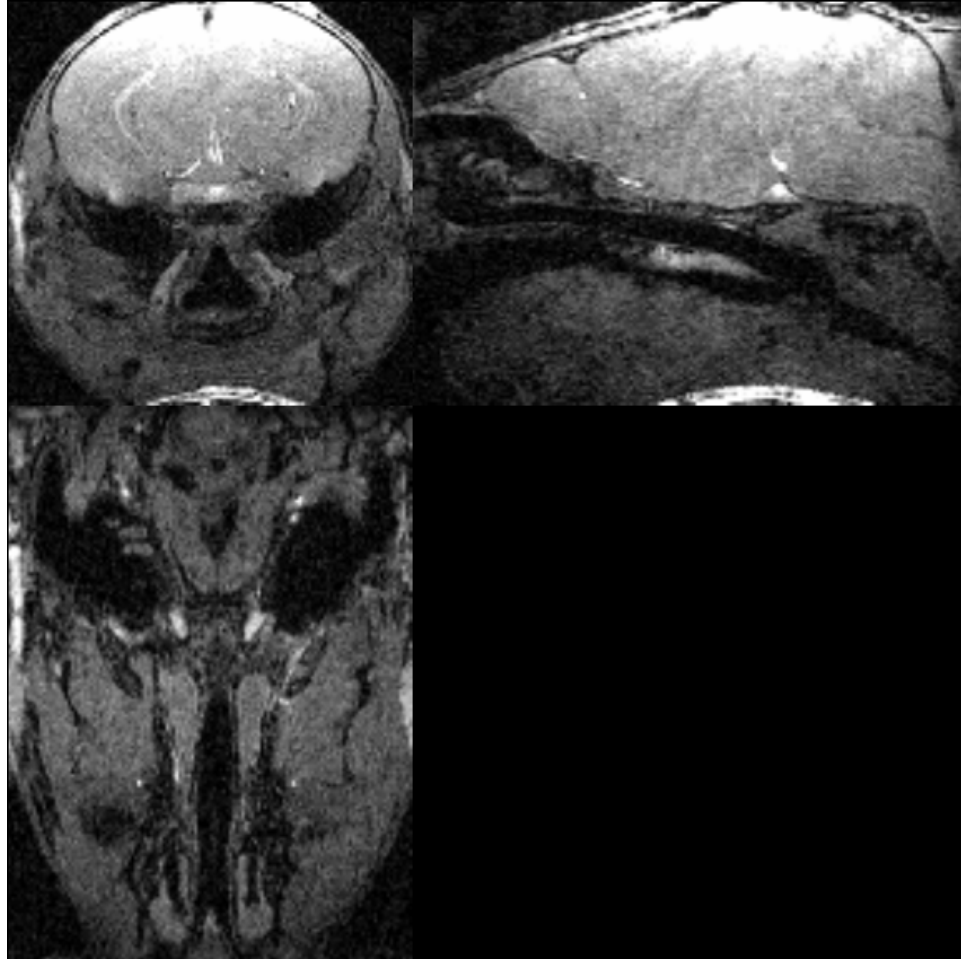


Figure 4.1: MRI volume:(a) Coronal view, (b) Sagittal view, (c) Axial View

4.1.2 Blockface and Histological Images

BlockFace Images The blockface images are produced by a series of procedures. Just after the MRI scan of the brain the rat infected with HIV-1 is sacrificed. Then the brain of the animal is removed with utmost care so that the intact shape of the brain is preserved as much as possible. The brain is put in an upside down position in a trough of paraffin and it is fixed. The entire brain fixed in paraffin is held in a clamp and with a precise slicing tool the brain is sliced into layers in the coronal plane at an interval of only $150\mu m$. Images of each of these slices are taken

which are known as the Blockface Images and they are shown below in the figure 4.2. Each of these slices are taken in such a way that they can be stacked up in 3D to regenerate the original brain volume and this property we will utilize when we use 3D alignment and registration technique to register the original brain volume and MRI volume in 3D.

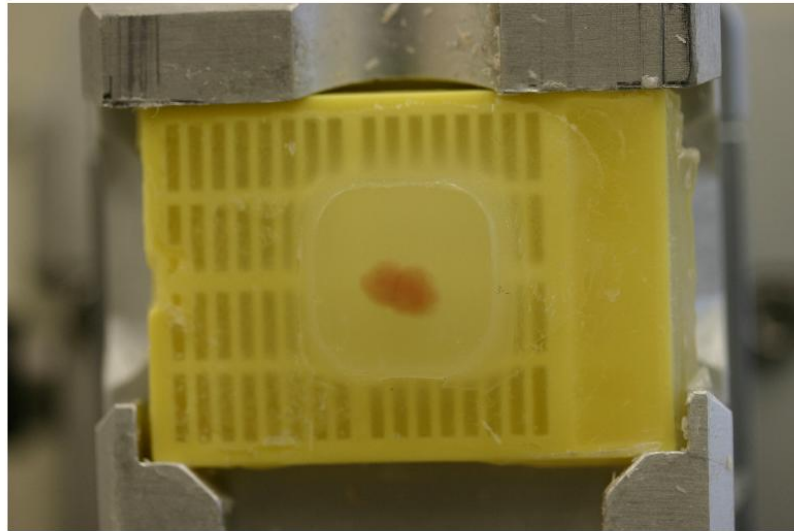


Figure 4.2: Blockface Image of the brain fixed in paraffin

Histological Images The blockface images thus produced are stained with Prussian Blue and the Histological Slices are produced. These histological slices of the brain are kept under the microscope for further studies, the 3D volume aligned MRI images are re-sliced to match these histological slices and we apply Thin-Plate Spline warping technique for non-linear co-registration of the MRI and Histological slices. The figure 4.3 shows one Histological image slice thus produced.

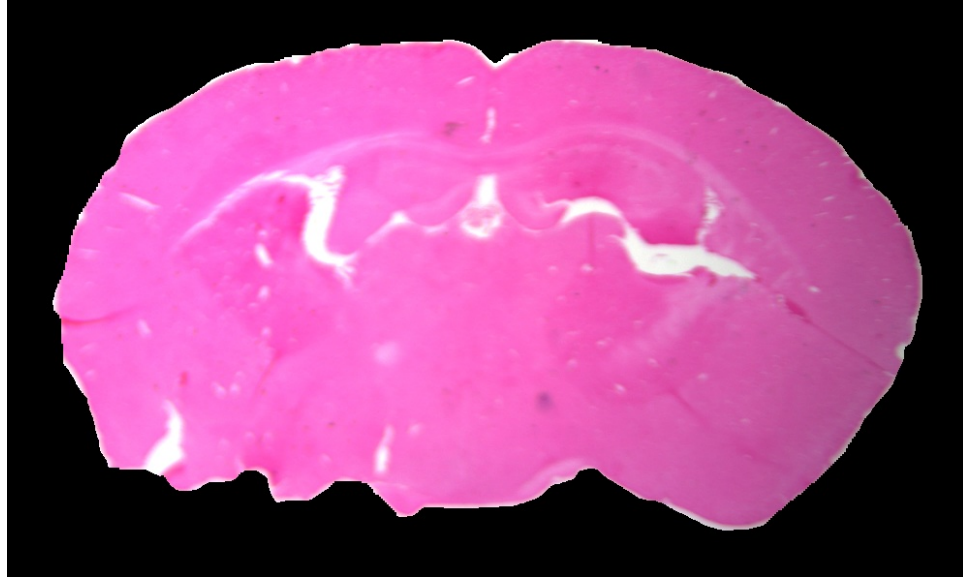


Figure 4.3: Histological Image slice

4.2 Results

Because this is an image processing project the results are mostly images that are generated by some image processing techniques. This project deals with several subsections like MRI image segmentation (4.4) with the application of level set evolution, blockface image segmentation (4.5) with canny edge detection principle, 3D reconstruction and alignment of MRI brain volume and Histological volume (??) and non-linear co-registration of MRI-histo image pairs (4.10) using thin plate spline technique. This section will consist mostly of the figures of input images and the processed images. The following figures show the results of different objectives of this project.

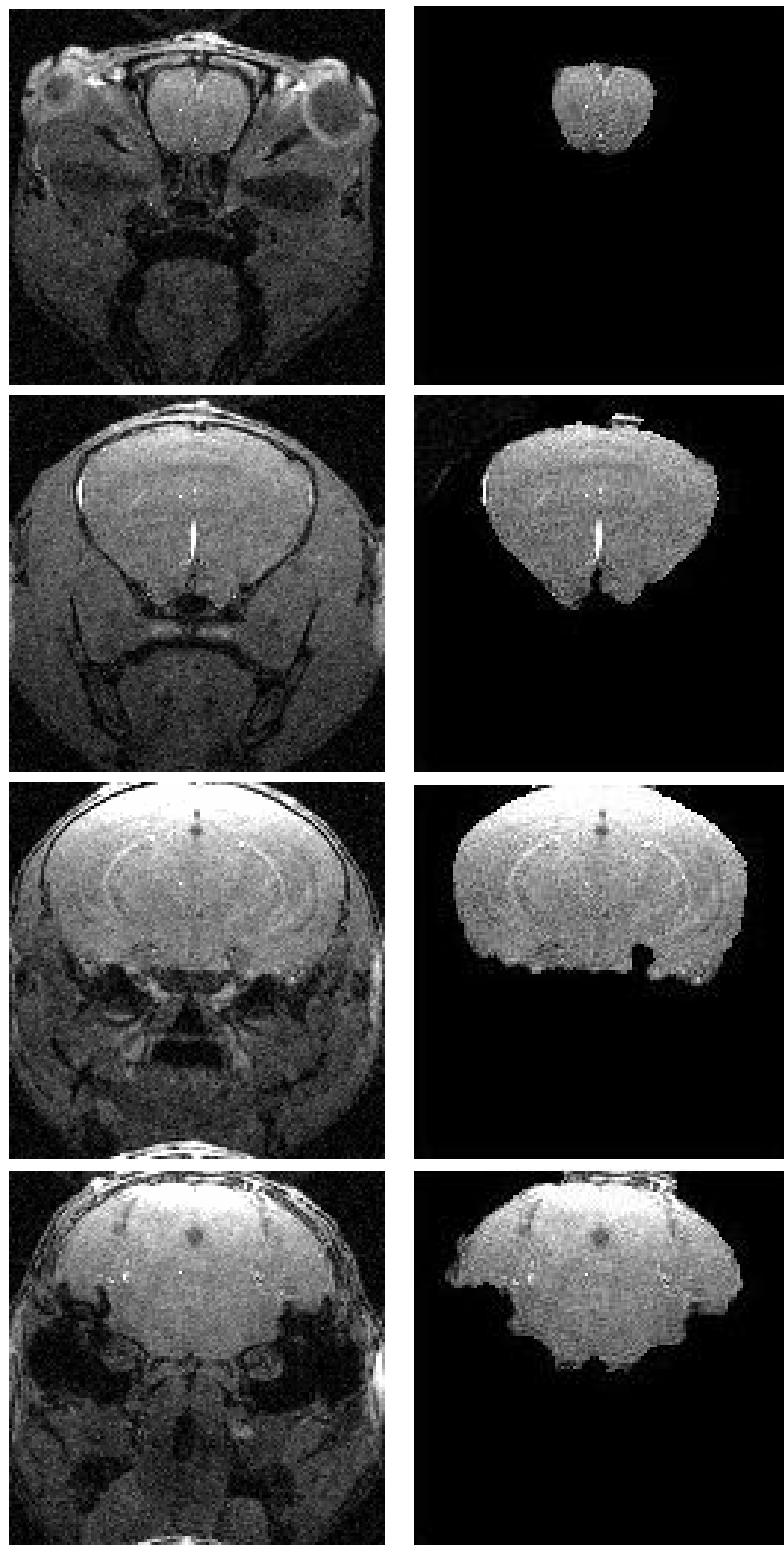


Figure 4.4: Level Set Evolution Application: Column(a) Whole head MRI slices
Column(b) Corresponding segmented brain sections

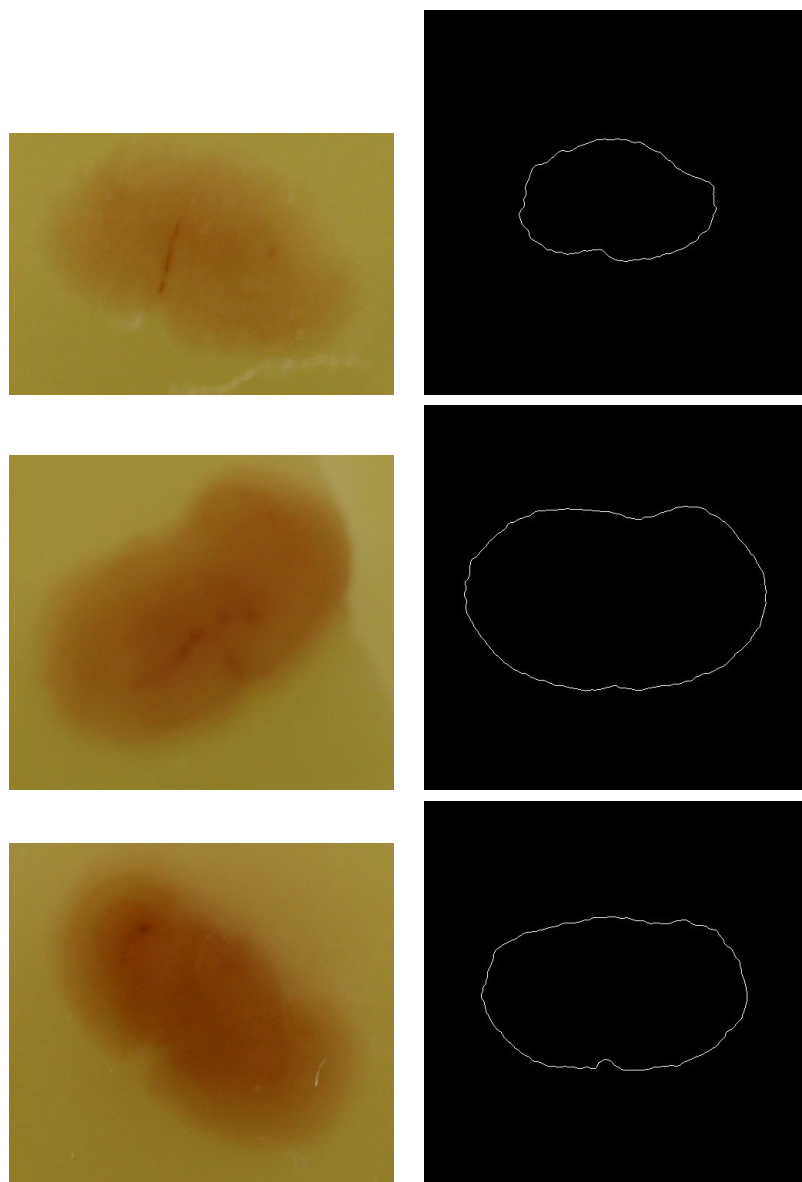


Figure 4.5: Blockface Image segmentation: Column(a) Blockface image slices
Column(b) Corresponding segmented and affine transformed brain sections

The segmentation of blockface slices were not perfect for all images in the dataset; the dataset is not quite as good as we expected. It is understandable that the sections were done physically with a cryostat, hence some slices were poorly imaged and resulted in poor segmented image quality. Some examples are shown in Figure (4.6)

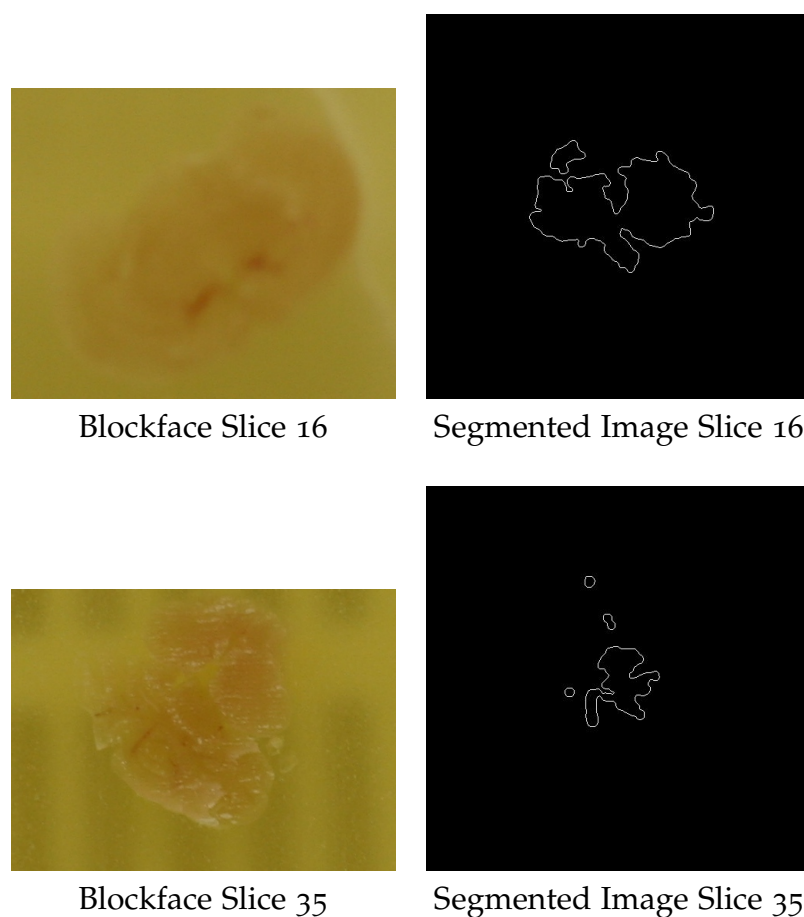


Figure 4.6: Poor Blockface Image segmentation examples

Because of the poor quality of the segmented image the entire brain volume could not be regenerated from the stack of blockface images. We checked the 3D alignment algorithm considering only a part of the brain that was regenerated. Figure 4.7 represents the MRI volume and the Blockface volume generated. The

volume aligned image is displayed in Figure 4.8. The volume representation in 2D images are difficult and hence Figure 4.9 shows only one slice of the MRI volume, corresponding slice of blockface volume and the volume aligned image slice. At this point the research is targeted to align the MRI image volume with the blockface image volume, it is not yet researched how to determine the transformation of the pixel values of the MRI volume to the aligned volume. In order to do the next section of the project that is Thin Plate Spline Registration of MRI and Histological image pairs we use a dataset of 10 sets of MRI-Histo pairs which are previously aligned. The results obtained from this step are shown in Figure 4.10. Three experienced technicians did the landmarking procedure on these sets of MRI-Histo images and the automatic landmarking procedure developed in this research is evaluated based on the Normalized Mutual Information measure of the resulting warped images obtained from the two procedures.

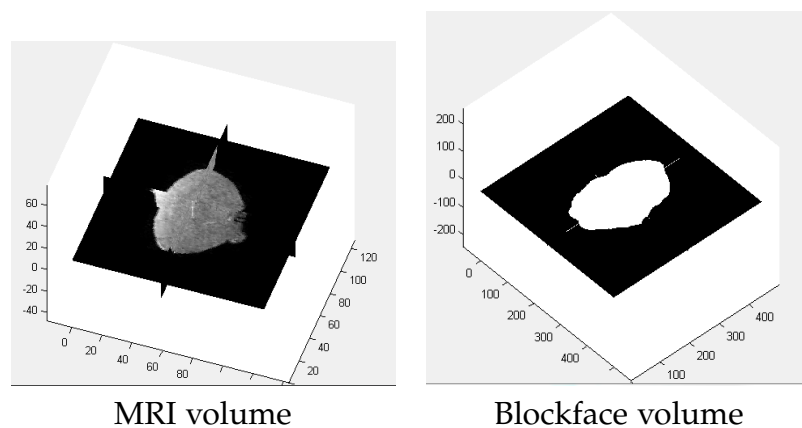


Figure 4.7: Representation of MRI and Blockface volume

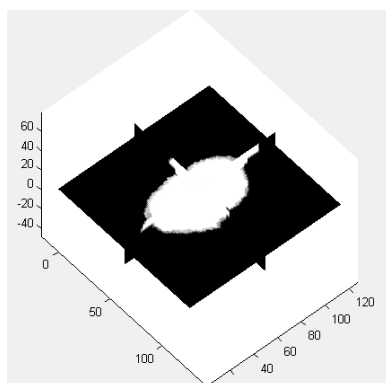
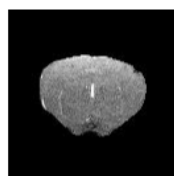


Figure 4.8: Representation of 3D aligned volume



MRI slice 20



Blockface slice 3



3D aligned slice 20

Figure 4.9: Representation of MRI and Blockface and 3D aligned slices

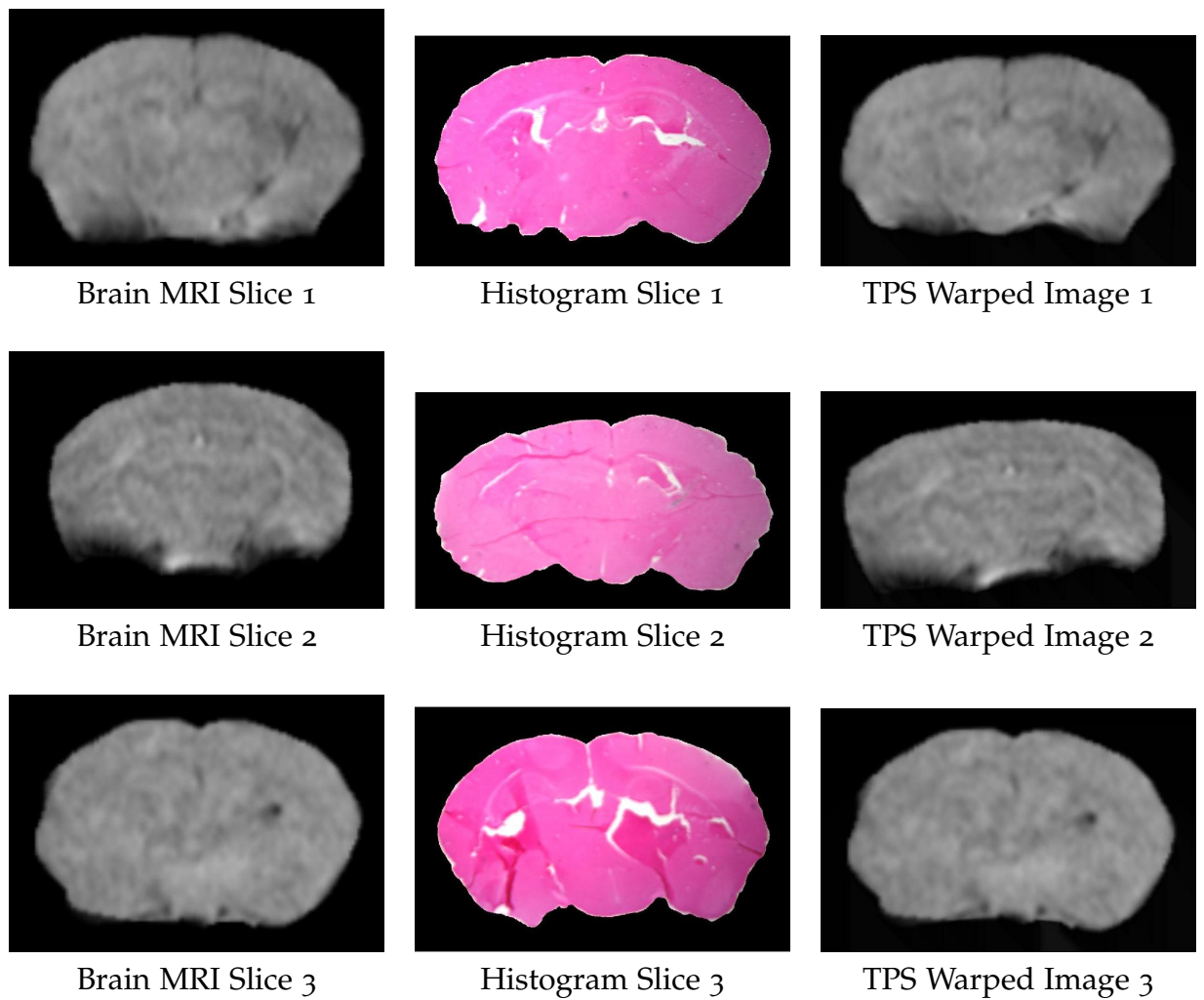


Figure 4.10: Thin Plate Spline(TPS) warping results of three MRI-Histological Slice pairs

4.3 Evaluation

In this section the data obtained from the automated landmarking system is directly compared against the results obtained from manual landmark selection procedures. The quality of the warped image and the Normalized mutual information index shows significant improvement over the manual techniques. Figure 4.11 , Figure 4.12 and Figure 4.13 show the comparative study of the warped images obtained from manual landmarking method 1, manual landmarking method 2, manual landmarking method 3 and the automatic landmarking method developed in this project. Table 4.1, Table 4.2 and Table 4.3 represent a list of source and target points on the MRI and Histology pair apart from the landmark points. The target points obtained from the automatic landmark methods are listed in the column 3 of each of the tables. This gives us another index of registration accuracy and evaluation of the automatic landmark method, *Target Registration Error* which is defined as

$$TRE = \frac{\sum_{i=1}^n |f(s_i) - t_i|}{n} \quad (4.1)$$

where n is the number of points apart from the landmark points that are considered for evaluation. f is the transformation i.e. Thin Plate Spline in this project. *Target Registration Error* is not used as an index in this project, it will be taken up as a future work. The Table 4.4 and Figure 4.14 represents the comparison of Normalized Mutual Information obtained from the automatic landmarking method and the manual methods.

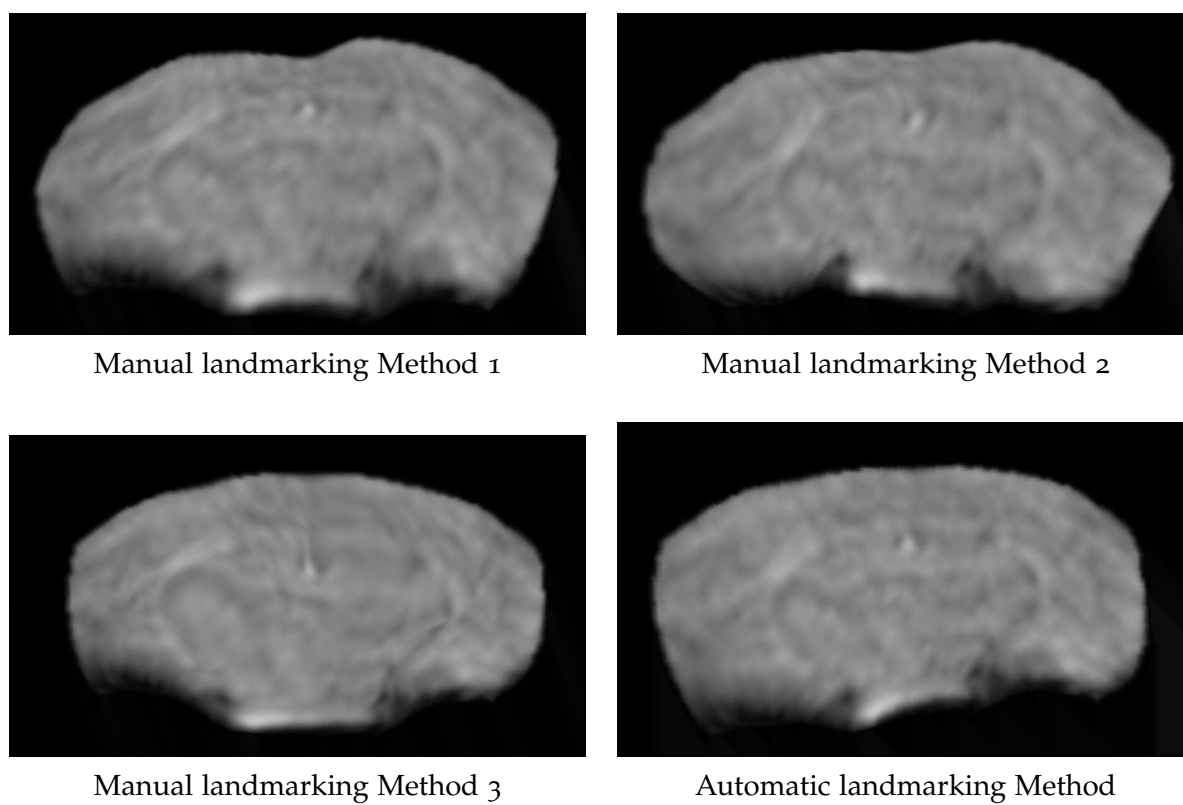
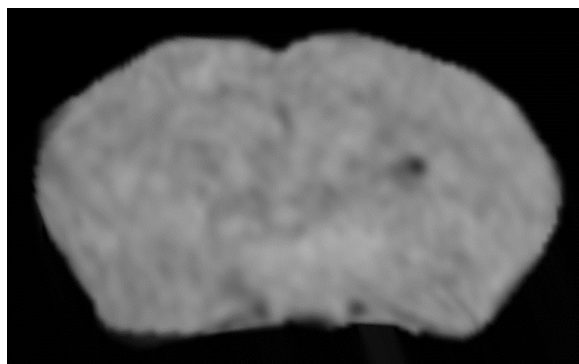
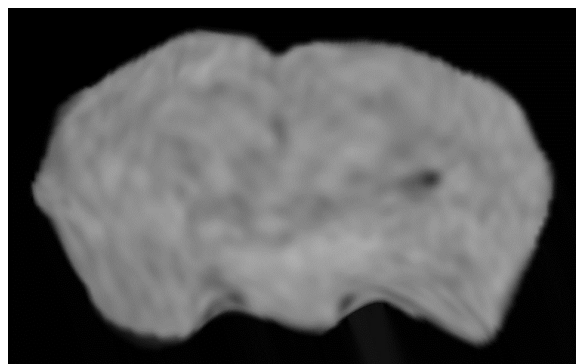


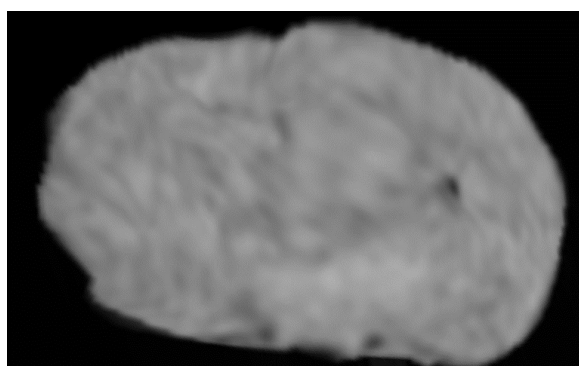
Figure 4.11: Comparison of Warped Images obtained from Manual Landmarking Methods and Automatic Landmarking Methods of Brain Slice 1



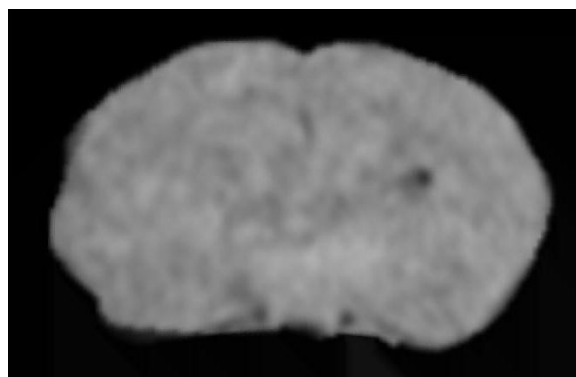
Manual landmarking Method 1



Manual landmarking Method 2



Manual landmarking Method 3



Automatic landmarking Method

Figure 4.12: Comparison of Warped Images obtained from Manual Landmarking Methods and Automatic Landmarking Methods of Brain Slice 2

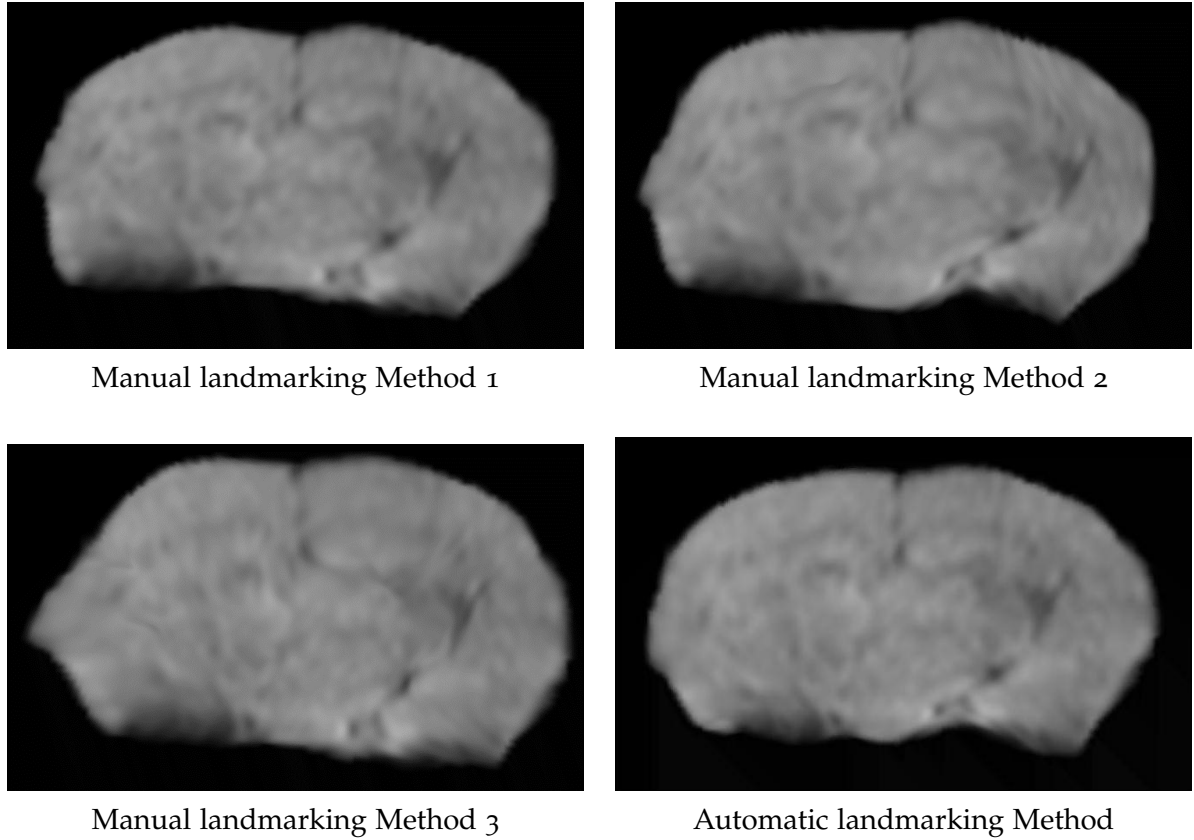


Figure 4.13: Comparison of Warped Images obtained from Manual Landmarking Methods and Automatic Landmarking Methods of Brain Slice 3

Table 4.1: Comparison of Target points on the Histological Image and Warped Points obtained from Experiment for particular Source Points (Set1)

Source Points		Target Points		Warped points	
X	Y	X	Y	X	Y
211.216667	90.04	425.406667	139.78	329.7	260.50
299.09	143.84	547.753333	235.673333	541.5	181.19
320.61	91.833333	607.273333	133.166667	544.1	150.95
191.49	97.213333	389.033333	146.393333	297.0	282.07
313.436667	39.826667	584.126667	47.193333	490.4	148.76

Table 4.2: Comparison of Target points on the Histological Image and Warped Points obtained from Experiment for particular Source Points (Set2)

Source Points		Target Points		Warped points	
X	Y	X	Y	X	Y
214.803333	91.833333	425.406667	143.086667	337.9	257.12
313.436667	93.626667	597.353333	133.166667	531.0	158.29
313.436667	39.826667	584.126667	47.193333	490.4	148.76
299.09	143.84	547.753333	235.673333	541.5	181.19
193.283333	95.42	392.34	149.7	299.2	279.91

Table 4.3: Comparison of Target points on the Histological Image and Warped Points obtained from Experiment for particular Source Points (Set3)

Source Points		Target Points		Warped points	
X	Y	X	Y	X	Y
270.396667	120.526667	494.846667	215.833333	466.5	205.70
265.016667	86.453333	501.46	133.166667	429.9	205.18
211.216667	91.833333	422.1	143.086667	331.0	260.80
401.31	163.566667	716.393333	252.206667	772.5	84.87
266.81	47	504.766667	67.033333	404.1	19.658
265.016667	321.38	478.313333	526.66	581.6	247.18

Table 4.4: Comparison of Normalized Mutual Information of Warped Brain Slice and Histological sections

Brain Slice	Manual Landmark process 1	Manual Landmark process 2	Manual Landmark process 3	Automatic Landmark process
Slice 1	0.191	0.1981	0.1508	0.6925
Slice 2	0.1677	0.1859	0.1544	0.6695
Slice 3	0.1901	0.1931	0.1426	0.5987

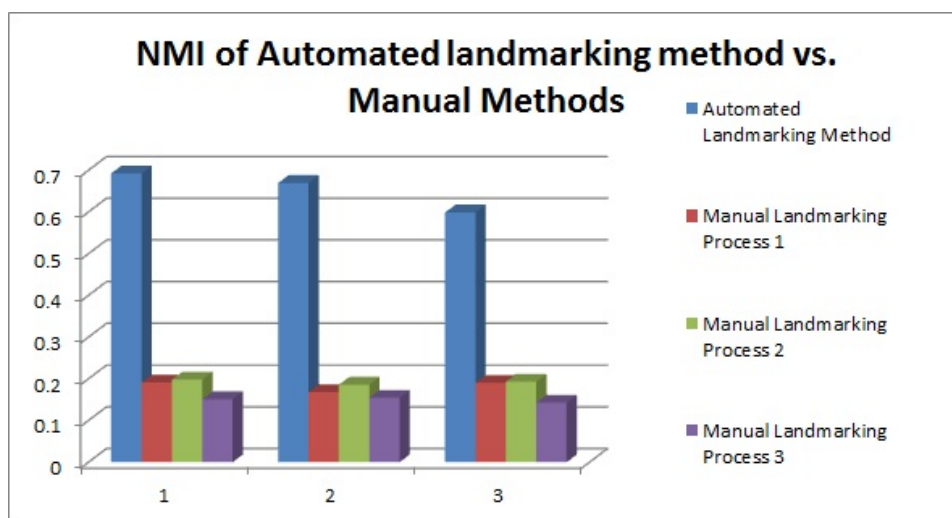


Figure 4.14: Comparison of Normalized Mutual Information of Warped Brain Slice and Histological sections

Chapter 5

Summary and Future Work

The research presented in this thesis addresses a challenging problem of Medical Image Registration of MR images and histology slices. This image processing technique is developed to track the growth of HIV-1 infection in rodent brain. Combining the data obtained from in-vivo MR imaging and the histological studies of the mouse brain can provide comprehensive knowledge about the growth of the disease. But the landmark selection and warping of the MR images with histological slices are mostly done manually which is tedious and error-prone. The main emphasis of this project was to develop a new approach towards automatic landmark selection techniques. The entire project can be considered as 4 distinct but related sections. First, the brain tissue is differentiated from its surrounding

non-brain tissues in MR image slices by level-set segmentation procedure. Then segmented brain images are stacked in 3D to reconstruct the in-vivo brain volume. The second aim of the project was to determine the global deformations between the MRI slices and the histological slices. In order to achieve that the concept of intermediate imaging technique of the brain was developed (blockface imaging in this case). The blockface brain slices is segmented from the blockface images using histogram equalization and canny edge detection principle. The blockface images are stacked in 3D to form a blockface volume. The third aspect of the project deals with the 3D reconstruction of MRI and blockface volumes and alignment of the two brain volumes to reduce the global deformation parameters and hence simplify the further registration procedure. After 3D alignment the MRI volume is re-sliced to match corresponding histological sections. The final step in the project was the application of Thin Plate spline Warping technique to get a non-linear registration between MRI and histological slices. The set of landmarks required for the coregistration procedure is selected automatically and the final number of landmarks used and the position of the landmarks are optimized automatically based on the maximization of Normalized Mutual Information between the warped image and the histological image.

Considering the time complexity of the optimization procedure it is not the best designed algorithm. The initial landmark points are defined arbitrarily as the centroid and 4 other points at right angles to each other on the brain boundary. Therefore the algorithm repeatedly counts the NMI of the warped image and the histological image and tries to determine the optimized location of the landmark initially determined. Suppose there are n number of landmarks which are optimized and the number of possible positions checked for NMI

maximization is k . Clearly there are k^n different combinations generated in this procedure which makes this algorithm of exponential time complexity. This makes the entire procedure highly computationally intensive. In order to deal with this inherent problem of the designed algorithm we have decided to use heuristic approach in the future work. A good algorithm to work with would be the Genetic Algorithm which votes for some specific arrangements out of the k^n different combinations based on some pre-determined screening procedure.

Bibliography

- [1] Image enhancement: Histogram equalization.
- [2] F. Akai, M. Maeda, K. Suzuki, S. Inagaki, H. Takagi, and N. Taniguchi. Immunocytochemical localization of manganese superoxide dismutase (mn-sod) in the hippocampus of the rat. *Neurosci Lett*, 115(1):19–23, Jul 17 1990. 0304-3940 (Print) Journal Article.
- [3] A. L. Alexander, J. E. Lee, M. Lazar, and A. S. Field. Diffusion tensor imaging of the brain. *Neurotherapeutics*, 4(3):316–29, Jul 2007. 1933-7213 (Print) Journal Article Research Support, N.I.H., Extramural Research Support, Non-U.S. Gov't Review.
- [4] D. C. Alexander and G. J. Barker. Optimal imaging parameters for fiber-orientation estimation in diffusion mri. *Neuroimage*, 27(2):357–67, Aug 15 2005. 1053-8119 (Print) Journal Article.
- [5] A. A. Ali, A. M. Dale, A. Badea, and G. A. Johnson. Automated segmentation of neuroanatomical structures in multispectral mr microscopy of the mouse brain. *Neuroimage*, 27(2):425–35, Aug 15 2005. 1053-8119 (Print) Journal Article.

- [6] P. R. Allegrini and C. Wiessner. Three-dimensional mri of cerebral projections in rat brain in vivo after intracortical injection of mncl₂. *NMR Biomed*, 16(5):252–6, Aug 2003. 0952-3480 (Print) Comparative Study Evaluation Studies Journal Article.
- [7] S. Alvestad, P. E. Goa, H. Qu, O. Risa, C. Brekken, U. Sonnewald, O. Haraldseth, J. Hammer, O. P. Ottersen, and A. Haberg. In vivo mapping of temporospatial changes in manganese enhancement in rat brain during epileptogenesis. *Neuroimage*, 38(1):57–66, Oct 15 2007. 1053-8119 (Print) Evaluation Studies Journal Article Research Support, Non-U.S. Gov't.
- [8] E. R. Anderson, J. Boyle, W. E. Zink, Y. Persidsky, H. E. Gendelman, and H. Xiong. Hippocampal synaptic dysfunction in a murine model of human immunodeficiency virus type 1 encephalitis. *Neuroscience*, 118(2):359–69, 2003. 0306-4522 (Print) Comparative Study Journal Article Research Support, U.S. Gov't, P.H.S.
- [9] F. Angenstein, H. G. Niessen, J. Goldschmidt, H. Lison, W. D. Altmann, E. D. Gundelfinger, and H. Scheich. Manganese-enhanced mri reveals structural and functional changes in the cortex of bassoon mutant mice. *Cereb Cortex*, 17(1):28–36, Jan 2007. 1047-3211 (Print) Journal Article Research Support, Non-U.S. Gov't.
- [10] I. Aoki, C. Tanaka, T. Takegami, T. Ebisu, M. Umeda, M. Fukunaga, K. Fukuda, A. C. Silva, A. P. Koretsky, and S. Naruse. Dynamic activity-induced manganese-dependent contrast magnetic resonance imaging (daim mri). *Magn Reson Med*, 48(6):927–33, Dec 2002. 0740-3194 (Print) Comparative Study Journal Article Research Support, Non-U.S. Gov't.

- [11] I. Aoki, Y. J. Wu, A. C. Silva, R. M. Lynch, and A. P. Koretsky. In vivo detection of neuroarchitecture in the rodent brain using manganese-enhanced mri. *Neuroimage*, 22(3):1046–59, Jul 2004. 1053-8119 (Print) Journal Article.
- [12] M. Aschner. Manganese homeostasis in the cns. *Environ Res*, 80(2 Pt 1):105–9, Feb 1999. 0013-9351 (Print) Journal Article Research Support, U.S. Gov't, P.H.S. Review.
- [13] M. Aschner. Manganese: brain transport and emerging research needs. *Environ Health Perspect*, 108 Suppl 3:429–32, Jun 2000. 0091-6765 (Print) Journal Article Research Support, U.S. Gov't, P.H.S. Review.
- [14] M. Aschner and J. L. Aschner. Manganese neurotoxicity: cellular effects and blood-brain barrier transport. *Neurosci Biobehav Rev*, 15(3):333–40, Fall 1991. Aschner, M Aschner, J L ES05223/ES/NIEHS NIH HHS/United States S07RR05394-26/RR/NCRR NIH HHS/United States Research Support, U.S. Gov't, P.H.S. Review United states Neuroscience and biobehavioral reviews *Neurosci Biobehav Rev*. 1991 Fall;15(3):333-40.
- [15] P. Bajcsy, S.C. LEE, A. Lin, and R. Folberg. Three-dimensional volume reconstruction of extracellular matrix proteins in uveal melanoma from fluorescent confocal laser scanning microscope images. *Journal of microscopy*, 221(1):30–45, 2006.
- [16] K. Boesen, K. Rehm, K. Schaper, S. Stoltzner, R. Woods, E. Lüders, and D. Rottenberg. Quantitative comparison of four brain extraction algorithms. *NeuroImage*, 22(3):1255–1261, 2004.

- [17] F.L. Bookstein. Principal warps: Thin-plate splines and the decomposition of deformations. *Pattern Analysis and Machine Intelligence, IEEE Transactions on*, 11(6):567–585, 1989.
- [18] L.G. Brown. A survey of image registration techniques. *ACM computing surveys (CSUR)*, 24(4):325–376, 1992.
- [19] J.F. Canny. Finding edges and lines in images. *Massachusetts Inst. of Tech. Report*, 1, 1983.
- [20] J. Chiverton, K. Wells, E. Lewis, C. Chen, B. Podda, and D. Johnson. Statistical morphological skull stripping of adult and infant mri data. *Computers in biology and medicine*, 37(3):342–357, 2007.
- [21] M.P. Deshmukh. A survey of image registration. *International Journal of Image Processing (IJIP)*, 5(3):245, 2011.
- [22] M. Droske, B. Meyer, M. Rumpf, and C. Schaller. An adaptive level set method for medical image segmentation. In *Information Processing in Medical Imaging*, pages 416–422. Springer, 2001.
- [23] Y. Liu et al. Ingress of blood-borne macrophages across the blood-brain barrier in murine hiv-1 encephalitis. *J Neuroimmunol*, 200(PMCID 2572762):41–52, 2008.
- [24] C. Fennema-Notestine, I.B. Ozyurt, C.P. Clark, S. Morris, A. Bischoff-Grethe, M.W. Bondi, T.L. Jernigan, B. Fischl, F. Segonne, D.W. Shattuck, et al. Quantitative evaluation of automated skull-stripping methods applied to contemporary and legacy images: Effects of diagnosis, bias correction, and slice location. *Human brain mapping*, 27(2):99–113, 2006.

- [25] Howard E. Gendelman. *The neurology of AIDS*. Oxford University Press, Oxford ; New York, 2nd edition, 2005. edited by Howard E. Gendelman ... [et al.]. ill. ; 29 cm.
- [26] M. Ghafouri, S. Amini, K. Khalili, and B. E. Sawaya. Hiv-1 associated dementia: symptoms and causes. *Retrovirology*, 3:28, 2006. 1742-4690 (Electronic) Journal Article Research Support, N.I.H., Extramural Review.
- [27] X. Han, C. Xu, and J.L. Prince. A topology preserving level set method for geometric deformable models. *Pattern Analysis and Machine Intelligence, IEEE Transactions on*, 25(6):755–768, 2003.
- [28] SW Hartley, AI Scher, ESC Korf, LR White, and LJ Launer. Analysis and validation of automated skull stripping tools: a validation study based on 296 mr images from the honolulu asia aging study. *NeuroImage*, 30(4):1179–1186, 2006.
- [29] D.L.G. Hill, P.G. Batchelor, M. Holden, and D.J. Hawkes. Medical image registration. *Physics in medicine and biology*, 46:R1, 2001.
- [30] M. A. Jacobs, J. P. Windham, H. Soltanian-Zadeh, D. J. Peck, and R. A. Knight. Registration and warping of magnetic resonance images to histological sections. *Med Phys*, 26(8):1568–78, Aug 1999. 0094-2405 Journal Article.
- [31] M.A. Jacobs, J.P. Windham, H. Soltanian-Zadeh, D.J. Peck, and R.A. Knight. Registration and warping of magnetic resonance images to histological sections. *Medical physics*, 26:1568, 1999.
- [32] M. Kaul, J. Zheng, S. Okamoto, H. E. Gendelman, and S. A. Lipton. Hiv-1 infection and aids: consequences for the central nervous system. *Cell Death*

Differ, 12 Suppl 1:878–92, Aug 2005. 1350-9047 (Print) Journal Article Research Support, N.I.H., Extramural Research Support, Non-U.S. Gov't Research Support, U.S. Gov't, P.H.S. Review.

- [33] D.J. Kroon and C.H. Slump. Mri modalitiy transformation in demon registration. In *Biomedical Imaging: From Nano to Macro, 2009. ISBI'09. IEEE International Symposium on*, pages 963–966. IEEE, 2009.
- [34] C. Li, C. Xu, C. Gui, and M.D. Fox. Level set evolution without re-initialization: A new variational formulation. In *Computer Vision and Pattern Recognition, 2005. CVPR 2005. IEEE Computer Society Conference on*, volume 1, pages 430–436. Ieee, 2005.
- [35] Y. Liu, M.G. Uberti, H. Dou, R. Banerjee, C.B. Grotepas, D.K. Stone, B.E. Rabinow, H.E. Gendelman, and M.D. Boska. Ingress of blood-borne macrophages across the blood-brain barrier in murine hiv-1 encephalitis. *Journal of neuroimmunology*, 200(1):41–52, 2008.
- [36] Z. Ma, J.M.R. da Silva Tavares, and R.M.N.J. Jorge. A review on the current segmentation algorithms for medical images. *IMAGAPP 2009*, 2009.
- [37] D. MacDonald, N. Kabani, D. Avis, and A.C. Evans. Automated 3-d extraction of inner and outer surfaces of cerebral cortex from mri. *NeuroImage*, 12(3):340–356, 2000.
- [38] C.R. Maurer and J.M. Fitzpatrick. A review of medical image registration. *Interactive image-guided neurosurgery*, pages 17–44, 1993.
- [39] C.R. Meyer, B.A. Moffat, K. Kuszpit, P.L. Bland, TL Chenevert, A. Rehemtulla, and BD Ross. A methodology for registration of a histological slide and in

- vivo mri volume based on optimizing mutual information. *Molecular imaging*, 5(1):16, 2006.
- [40] E. Nadernejad, S. Sharifzadeh, and H. Hassanpour. Edge detection techniques: Evaluations and comparisons. *Applied Mathematical Sciences*, 2(31):1507–1520, 2008.
- [41] MJD Powell. The uniform convergence of thin plate spline interpolation in two dimensions. *Numerische Mathematik*, 68(1):107–128, 1994.
- [42] S. Price. Edges: The canny edge detector. 1996.
- [43] K. Rohr, M. Fornefett, and H. Stiehl. Approximating thin-plate splines for elastic registration: Integration of landmark errors and orientation attributes. In *Information Processing in Medical Imaging*, pages 252–265. Springer, 1999.
- [44] K. Rohr, M. Fornefett, and HS Stiehl. Spline-based elastic image registration: integration of landmark errors and orientation attributes. *Computer Vision and Image Understanding*, 90(2):153–168, 2003.
- [45] J.A. Sethian. Fast marching methods. *SIAM review*, pages 199–235, 1999.
- [46] M. Soret, S.L. Bacharach, and I. Buvat. Partial-volume effect in pet tumor imaging. *Journal of Nuclear Medicine*, 48(6):932–945, 2007.
- [47] J.P. Thirion. Image matching as a diffusion process: an analogy with maxwell’s demons. *Medical image analysis*, 2(3):243–260, 1998.
- [48] MG Uberti, Y. Liu, H. Dou, R.L. Mosley, H.E. Gendelman, and M. Boska. Registration of in vivo mr to histology of rodent brains using blockface imaging. In *Proc Soc Photo Opt Instrum Eng*, volume 7262, pages 726213–726211, 2009.

- [49] M. Whitbeck and H. Guo. Multiple landmark warping using thin-plate splines. *IPCV'06*, pages 256–263, 2006.
- [50] H. Zaidi, T. Ruest, F. Schoenahl, and M.L. Montandon. Comparative assessment of statistical brain mr image segmentation algorithms and their impact on partial volume correction in pet. *Neuroimage*, 32(4):1591–1607, 2006.
- [51] B. Zitova and J. Flusser. Image registration methods: a survey. *Image and vision computing*, 21(11):977–1000, 2003.